Laser Spectroscopy of $^3A_2 \rightarrow {}^1A_1$ Phosphorescence of Sulphur Dioxide

by

H. M. Abdulkader Dastageer

A Thesis Presented to the

FACULTY OF THE COLLEGE OF GRADUATE STUDIES

KING FAHD UNIVERSITY OF PETROLEUM & MINERALS

DHAHRAN, SAUDI ARABIA

In Partial Fulfillment of the
Requirements for the Degree of

MASTER OF SCIENCE

In

PHYSICS

December, 1993

Order Number 1360413

Laser spectroscopy of $^3A_2 \rightarrow ^1 A_1$ phosphorescence of sulphur dioxide

Dastageer, H. M. Abdulkader, M.S.

King Fahd University of Petroleum and Minerals (Saudi Arabia), 1993

U·M·I
300 N. Zeeb Rd.
Ann Arbor, MI 48106

LASER SPECTROSCOPY OF $^3A_2 \rightarrow {}^1A_1$ PHOSPHORESCENCE OF SULPHUR DIOXIDE

BY

H. M. ABDULKADER DASTAGEER

A Thesis Presented to the

FACULTY OF THE COLLEGE OF GRADUATE STUDIES

KING FAHD UNIVERSITY OF PETROLEUM & MINERALS

DHAHRAN, SAUDI ARABIA

In Partial Fulfillment of the
Requirements for the Degree of

MASTER OF SCIENCE

In

PHYSICS

DECEMBER, 1993

KING FAHD UNIVERSITY OF PETROLEUM AND MINERALS

DHAHRAN, SAUDI ARABIA.

COLLEGE OF GRADUATE STUDIES

This thesis, written by **Mr. H.M. ABDULKADER DASTAGEER** under the direction of his thesis advisor and approved by his thesis committee, has been presented to and accepted by the Dean of the College of Graduate Studies, in partial fulfillment of the requirements for the degree of **MASTER OF SCIENCE** in Physics.

Thesis committee

Dr. Fida Al - Adel
(Thesis advisor)

Dr. Ezzat Higazi
(Thesis co - advisor)

Dr. Riazuddin
(Member)

Dr. Abdulaziz Al - Suwaiyan
(Member)

Dr. Abdulaziz Al - Harthi
Chairman, Department of Physics.

Dr. Ala H. Al - Rabeh
Dean, College of Graduate Studies.

Date: ٢١/٧/١٤٢٥

This thesis is dedicated to my beloved
Maternal and Paternal grand fathers

ACKNOWLEDGMENT

Praise be to Allah, Who bestowed His boundless mercy on me to accomplish this work. May Allah's peace and blessing be upon His mighty messenger Prophet Mohammed, who inspired the humanity to seek knowledge wherever it is available.

Acknowledgment is due to King Fahd University of Petroleum and Minerals.

I record my profound sense of gratitude and sincere appreciation to my thesis advisor and committee chairman Dr. Fida Al - Adel, who developed in me a natural taste for the laser spectroscopy through his valuable guidance and constant help to carry out this work. I also express my deep gratitude to my co - advisor Dr. Ezzat Higazi, for his valuable guidance and constant help to accomplish this work. I wish to thank my committee members Dr. Riazuddin and Dr. Abdulaziz Al- Suwaiyan for their valuable suggestions, comments and encouragement. I would like to thank Mr. Abdulla Hamdan who trained me in the laser and supersonic jet system.

I also express my gratitude to each and every member of Laser research program and Physics department for their moral support and well wishes. I acknowledge the help rendered by the staff of KFUPM main library. Finally, I am grateful to my colleagues and friends who made my stay in KFUPM a memorable experience.

TABLE OF CONTENTS

LIST OF TABLES

Table

LIST OF FIGURES

Figure *page*

THESIS ABSTRACT

NAME OF THE STUDENT : H.M.ABDULKADER DASTAGEER

TITLE OF STUDY : LASER SPECTROSCOPY OF $^3A_2 \rightarrow {}^1A_1$ PHOSPHORESCENCE OF SULPHUR DIOXIDE

MAJOR FIELD : PHYSICS

DATE OF DEGREE : DECEMBER 1993

Supersonic jet beam of SO_2 seeded in Ar was excited by 3021Å laser radiation and the resulting luminescence spectrum was recorded in the 3060 - 5000 Å range. At very low SO_2 concentration two different phosphorescence spectra were distinguished from the F - band resonance fluorescence spectrum when proper optical alignment was used. One phosphorescence spectrum was recognized as the $^3B_1 \rightarrow {}^1A_1$ band system while the second was assigned as the previously undetected $^3A2 \rightarrow {}^1A_1$ band system. The distinction between the two band systems was based mainly on the observation that each system reached vibrational equilibrium at SO_2 pressure different from the other . Five progressions of energy separation 955 cm^{-1} were identified as ν_1' progressions of $^3A_2$ state. The zero order values for ν_2' is around 417cm^{-1} and ν_3' is around 1062 cm^{-1}, on the other hand, were estimated from a tentative vibrational analysis of the resulting $^3A_2 \rightarrow {}^1A_1$ phosphorescence spectrum. The formation mechanism of the triplet molecules and the possible internal conversion between the $^3A_2$ and $^3B_1$ states are also discussed.

MASTER OF SCIENCE DEGREE

KING FAHD UNIVERSITY OF PETROLEUM AND MINERALS

Dhahran, Saudi Arabia

December, 1993

خلاصة الرسالة

اسم الطالب : عبد القادر داستاجير

عنوان البحث : « الدراسه الطيفيه بواسطة الليزر للانبعاث $^3A_2 \longrightarrow {}^1A_1$ من جزيء ثاني أكسيد الكبريت »

القسم : الفيزياء

التاريخ : كانون اول ١٩٩٣

لقد تم إثاره الحزم الجزيئيه الفوق صوتيه لجزيء ثاني أكسيد الكبريت الممزوج بغاز الأرجون باستخدام طول موجة الليزر (٣٠٢١ أنجستروم) . وقد سُجل طيف الانبعاث في المدى (من ٣٠٦٠ إلى ٥٠٠٠ انجستروم) ، وعند استخدام نسبه قليله جداً من جزيئات ثاني أكسيد الكبريت تم تمييز نوعين مختلفين للانبعاث طويل الاجل من طيف الانبعاث الرنيني للشريط أو المدى الطيفي " F " ، وذلك باستخدام مسار مناسب لأشعة الليزر . وأحد هذين النوعين الذى يمكن التعرف عليه هو $^3B_1 \longrightarrow {}^1A_1$. أما النوع الثاني فهو الانبعاث $^3A_2 \longrightarrow {}^1A_1$ والذي لم يتم رؤيته من قبل . ولقد ارتكز التمييز بين هذين النظامين (الانبعاثين) على المشاهده بأن كلا النظامين يصل الى حالة التوازن الاهتزازى بنسب مختلفة من ثاني أكسيد الكبريت . وقد تم التعرف أيضاً على خمسة مجموعات من الخطوط الطيفيه التابعه للشكل أو الوضع « v_1 » للمستوى الالكترونى $^3A_2$ والتي يفصل بين خطوطها طاقه مقدارها « ٩٥٥سم$^{-1}$ » . ومن ناحية أخرى تم تقريب القيمه الصفريه لطاقة الوضعين v_2, v_3 بـ (١٠٦٢ ، ٤١٧ سم$^{-1}$) وذلك من خلال التحليل المبدئي لطيف الانبعاث طويل الاجل ($^3A_2 \longrightarrow {}^1A_1$) كما تم مناقشة ميكانيكيه تكوين الجزيئات الثلاثيه واحتمال التغيير الداخلي بين المستويين الالكترونيين $^3B_1$ و $^3A_2$.

درجة الماجستير في العلوم

جامعة الملك فهد للبترول والمعادن

الظهران - المملكة العربية السعودية

كانون اول ١٩٩٣

CHAPTER I

INTRODUCTION

Spectroscopy may be defined as the study of interaction of electromagnetic waves with matter. The fact that the molecules possess quantized internal energy levels and that this enables them to absorb and emit electromagnetic radiation at discrete frequencies is the basis of molecular Spectroscopy.

Over the past three decades much information has accumulated on the properties of the excited electronic states of sulfur dioxide [1]. While at first this was a purely an academic problem in the ultraviolet spectroscopy, the demonstration that the excited SO_2 was much more reactive than the ground state spurred a later practical interest in the assessment of the photo chemistry of SO_2 in atmosphere.

The absorption spectrum of SO_2 has three main regions [2] of absorption: 1) 1650 - 2400 Å (Second Allowed Band) 2) 2400 - 3400 Å (First Allowed Band) 3) 3400 - 4000 Å (Forbidden Band). Among these three band systems, the first allowed band attracted the attention of many workers because of the inherent spectroscopic complexity in this region. Based on circumstantial evidence Herzberg [3] assigned the 2400 - 3400 Å

absorption as the $^1B_1 \leftarrow {}^1A_1$ transition, which was ruled out by the rotational analysis by Hamada and Merrer [4] in this spectral region. Hamada and Merrer confirmed that this absorption band is due to electronically forbidden $^1A_2 \leftarrow {}^1A_1$ transition, which was made allowed by Herzberg - Teller coupling through the antisymmetric stretch normal coordinates. Subsequent work on this region by Hamada and Merer [5] revealed that, $^1A_2 \leftarrow {}^1A_1$ transition alone can not explain all recognizable band structures of the first allowed band system. They pointed out that, besides $^1A_2 \leftarrow {}^1A_1$ transition, $^1B_1 \leftarrow {}^1A_1$ transition also appears only as a background of weak absorption. Thus they could account for all analyzable bands in the system.

Emission spectra of SO_2 were recorded by a few workers. Strickler and Howell [2] measured the luminescence spectrum of SO_2 in a closed cell when excited with wavelengths at 2894, 2967, 3021 and 3126-3132 Å and reported that at the low pressure of SO_2 inside the cell, only fluorescence spectrum was observed and the fluorescence quantum yield approached 1.0 at zero pressure in agreement with an independent report by Mettee [6]. Later work by Rao and Calvert [7] revealed that the fluorescence quantum yield at zero pressure was well below 1.0, ranging from 0.55 at the excitation wavelength 2650 Å to 0.061 at 3020 Å, which is quite contrary to the results obtained by Strickler and Howell [2]. Subsequently, in an elegant study of SO_2 fluorescence, Brus and McDonald[8,9] pointed out that the conclusions of Rao and Calvert, that the

fluorescence quantum yield less than unity at zero pressure was invalid because their experimental cell was very small and wall deactivation was occurring at low pressures. Brus and McDonald therefore agreed with Mettee that the fluorescence quantum yield approaches to one at zero pressures.

Brus and McDonald through the same work [8,9] also pointed out that the decay of SO_2 fluorescence was a double exponential decay and their work revealed that the emitted fluorescence has two different life times. They assigned the long lived fluorescence as the one originating from $^1A_2$ state and the short lived fluorescence as the one from $^1B_1$ state. The wavelength resolved study of Caton and Gangadharan [10] indicated that the fluorescence spectra of excited long lived and short lived species were identical, however, they assigned both as from $^1B_1$, one of which is strongly Renner coupled to the ground state to be short lived emission and the other one which is weakly Renner coupled to the ground state to be the long lived emission. The long lived $^1B_1$ state is coupled to the triplet manifold through the spin - orbit interaction, therefore it is possible that the $^3B_1$ molecules are formed through intersystem crossing.

Phosphorescence from the $^3B_1$ state is also seen when the absorption is into the first allowed band[11]. As mentioned before, some of the absorption, especially in the 3000 - 3300 Å region is directly to $^1B_1(L)$, which is coupled to the triplet manifold. Presumably the excitation can cross over to the $^3B_1$ state to produce phosphorescence. At low pressures,

Strickler and Howell [2] and Mettee [6] found that the phosphorescence disappeared below 20 mtorr. This suggests that the first order intersystem crossing from $^1B_1(L)$ to $^3B_1$ may not occur. However in both studies the diffusional loss of $^3B_1$ to the walls could be important at low pressures [12] because of the long lifetime of $^3B_1$. In a paper by Caton and Gangadharan, the phosphorescence quantum yield was measured for pressure from 0.6 mtorr to 200 mtorr. Excitation wavelengths at 3131, 3021, 2967, and 2894 Å were used. The emission yield drops as the pressure is reduced from 20 mtorr to approximately 3 mtorr. For incident radiation at 2894 and 2967Å (where $^1B_1(L)$ is not strongly coupled to the triplet manifold), the further reduction below 4 mtorr continues to reduce the phosphorescence yield towards zero. However, for 3021 and 3131 Å incident radiations (where the $^1B_1(L)$ is strongly coupled to the triplet manifold), a further reduction in pressure below 4 mtorr enhances the phosphorescence yield. No explanation of this phenomenon has ever been suggested.

No phosphorescence other than that associated with the decay of $^3B_1$ level has so for been identified. However, the prescence of $^3A_2$ was predicted by noticing that the measured $^3B_1$ phosphorescence spectra showed unexpected Franck - Condon factors in the 3500 - 3750 Å region[13]. The failure to detect $^3A_2 \longrightarrow {}^1A_1$ phosphorescence directly in these studies may be rationalized as due to two reasons. First the phosphorescence signal is relatively very weak such that it is swamped out by the stronger fluorescence background at high pressure, and second a

large fraction of long lived $^3A_2$ molecules suffer from deexcitation at the walls of the cell as they diffuse out at the low pressure condition.

In the present thesis we investigate wavelength resolved luminescence spectrum in a supersonic jet when excited by 3021 Å laser radiation [14]. This wavelength was chosen in particular, because, it lies within the region where $^1B_1(L)$ is strongly coupled to the triplet manifold, and also because it is the same excitation wavelength that shows upturn phenomenon in the phosphorescence yield as reported by Caton and Gangadharan [10]. The varying values of the molecular density in the closed cell experiments were simulated in supersonic jet by changing the laser to nozzle distance (X) and $[SO_2]/[Ar]$ ratio. Such sensitive controls allow us to reach low SO_2 densities that correspond to SO_2 partial pressure as low as 0.1 mtorr and to detect for the first time the $^3A_2 \longrightarrow {}^1A_1$ phosphorescence. In our experiment both the $^3A_2$ and $^3B_1$ signal showed considerable dependence on geometrical alignment of the exciting beam and detecting system at low SO_2 concentration, which indicated that triplet molecules had in fact undergone significant diffusion within the expanded jet. However because of the absence of the walls and the large velocity component that molecules gain along the axis of the expanded jet, the diffused triplet molecules seemed to have been confined inside a limited volume around the exciting laser beam such that their decay could be detected under optimum geometrical alignment and proper excitation / detection delay.

An attempt has been made to analyze $^3A_2 \longrightarrow {}^1A_1$ band system and to discuss the possible formation mechanism for $^3A_2$ and $^3B_1$ molecules based on the pure electronic states as predicted in theory. A possible explanation for the upturn phenomenon[10] in $^3B_1$ phosphorescence quantum yield is also presented in the light of our results.

CHAPTER II

THEORY

2.1 Structure of SO_2

SO_2 is a nonlinear symmetric triatomic molecule with equilibrium bond angle θ_e = 119.329(2) and bond length r_e = 1.43080(1) Å in the ground state[15]. The structure and the bonding of the gaseous SO_2 is described by mesomeric structure shown in figure 2.1 [16]. The percentage of individual structure in the molecule is not known for certain, but mesomeric structure II is beleived to represent the ground state the best. The bond angle and bond length of SO_2 in the excited electronic states are different. These values for some of the electronic states were estimated by many workers[1].

In SO_2, the sulphur atom and both of the two oxygen atoms have six valance electron in the outer most shell. The two valance electrons of sulphur atom make a double bond with the two valance electrons of one of the two oxygen atoms. The same double bonding takes place between the sulphur and other oxygen atom also. The resulting structure is represented by structure II of the mesomeric structure. Another possibility is one bond of one of the double bonds in structure II can break and the two electrons

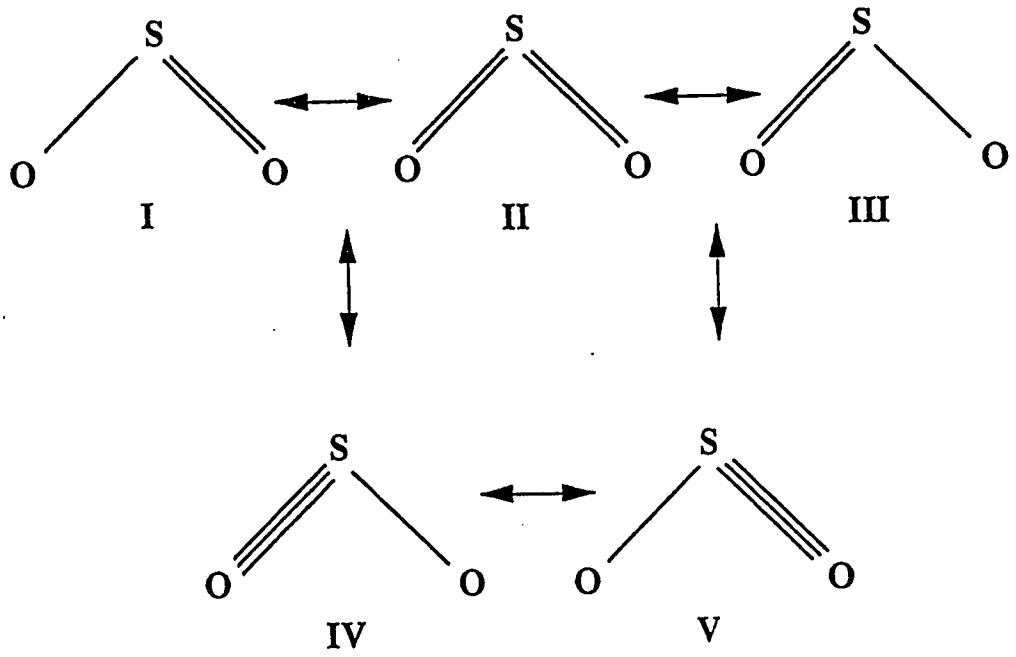

Figure : 2.1 Mesomeric structure of Sulphur dioxide

The lines in the figures indicates single double and triple bonds

of the broken bond will move towards the oxygen atom because of the higher electronegativity of oxygen atom than the sulphur atom. The result will be one single bond with one oxygen atom and another double bond with other oxygen atom which is represented by mesomeric structures I & III. Yet another possibility is one pair of electrons in the oxygen atom in structure II forms a bond with sulphur atom resulting in triple bond. At the same time one bond in other double bond will break and the electron pair will be transferred to the concerned oxygen atom. The resulting structure is represented by mesomeric structures IV & V.

2.2 Symmetry and the group theory of SO_2

In addition to the identity symmetry, SO_2 molecule possesses C_{2z} axis of symmetry, i.e. when SO_2 molecule is rotated 180^0 about C_{2z} axis as shown in the figure 2.2, the molecule remains unchanged. Also it has two planes of symmetry $\sigma_v(XZ)$ and $\sigma_v(YZ)$, which include C_{2z} axis as shown in figure 2.2 [17], hence SO_2 molecule belongs to non degenerate C_{2v} point group. Each of the four symmetry elements of the C_{2v} group is a class by itself. So C_{2v} point group has four classes and hence four irreducible representations.

The character table of C_{2v} group is shown in table 2.1, a property such as a vibrational wave function of SO_2 may or may not preserve an element of symmetry. If it preserves the element on carrying

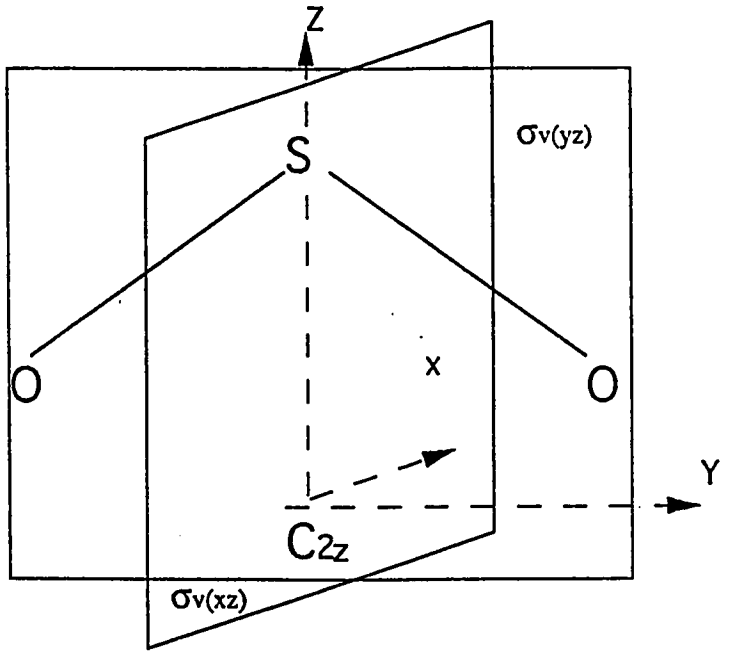

Figure : 2.2 C2z, σv(xz) and σv(yz) symmetry of SO2

Table 2.1 Character table of C2v group

C2v	I	C_2	$\sigma_{v(xz)}$	$\sigma_{v(yz)}$	
A_1	1	1	1	1	T_z
A_2	1	1	-1	-1	R_z
B_1	1	-1	1	-1	T_x, R_y
B_2	1	-1	-1	1	T_y, R_x

Table 2.2 Multiplication table of symmetry species

.	A_1	A_2	B_1	B_2
A_1	A_1	A2	B_1	B2
A_2	A_2	A_1	B_2	B_1
B_1	B_1	B_2	A_1	A_2
B2	B_2	B_1	A_2	A_1

out the corresponding symmetry operation, then the wave function is said to be symmetric with respect to that operation. For example σ_v has no effect on the wave function which we write as

$$\psi_v \xrightarrow{\sigma_v} (+1)\,\psi_v \qquad (2.2.1)$$

Therefore ψ_v is said to be symmetric with respect to σ_v. The only other possibility in a non degenerate point group is that the wave function may be changed on carrying out the operation. i.e.

$$\psi_v \xrightarrow{\sigma_v} (-1)\,\psi_v \qquad (2.2.2)$$

in which case we say that ψ_v is antisymmetric to σ_v. The (+1) of equation 2.1.1 and (-1) of equation 2.2.2 are known as the characters of, in this case ψ_v with respect to σ_v.

We have seen that any two of C_{2z} , $\sigma_v(XZ)$, $\sigma_v(YZ)$ elements may be regarded as generating elements. There are four possible combination of +1 and -1 characters with respect to these generating elements, +1 and +1, +1 and -1, -1 and +1 , -1 and -1 with respect to C_{2z} and $\sigma_v(XZ)$. These combinations are entered in column 3 and column 4 of the C_{2v} character table 3.1. The character with respect to the identity element I must always be +1 and, just as $\sigma_v(YZ)$ is the product of C_{2z} and $\sigma_v(XZ)$, the character with respect to $\sigma_v(YZ)$ is also the product of the

characters with respect to C_{2z} and $\sigma_v(XZ)$. Each of the four rows of the character table is called an irreducible representation of the group and for convenience each is represented by the symmetry species A_1, A_2, B_1, B_2. The A_1 species is said to be totally symmetric since all the characters are +1; the other three specie are non totally symmetric.

The symmetry species labels are conventional. A and B indicate symmetric or antisymmetric respectively with respect to C_{2z} and the subscript 1 and 2 indicate the symmetry or antisymmetry with respect to $\sigma_v(XZ)$. The sixth column of the character table indicates the symmetry species of translation (T) of the molecule along, and the rotation (R) about, the cartesian axes. The symbol Γ stands for the phrase " the symmetry species of " some operator, wave function etc.

$$\Gamma(T_x) = B_1 ; \quad \Gamma(T_y) = B_2 ; \quad \Gamma(T_z) = A_1$$

$$\Gamma(R_x) = B_2 ; \quad \Gamma(R_y) = B_1 ; \quad \Gamma(R_z) = A_2 \qquad (2.2.3)$$

The SO_2 molecule has three normal modes of vibration which will be discussed in detail in section 2.5. Using the C_{2v} character table the wave function ψ_v for each normal mode of vibration can easily be assigned to symmetry species. The character of the three vibrations under the operations C_{2z} and $\sigma_v(XZ)$ are respectively +1 and +1 for ν_1 and +1 and +1 for ν_2 and -1 and -1 for ν_3

$$\Gamma(\psi_{v_1}) = A_1 ; \quad \Gamma(\psi_{v_2}) = A_1 ; \quad \Gamma(\psi_{v_3}) = B_2 \qquad (2.2.4)$$

The direct product of the symmetric specie are listed in table 2.2. For example if SO_2 is vibrationally excited simultaneously with one quanta each of ν_1 and ν_3 then, the symmetry species of the wavefunction for this vibrational combination state is the product of symmetry species of the wave functions of ν_1 and ν_3 i.e.

$$\Gamma\psi_v = A_1 \times B_2 = B_1 \qquad (2.2.5)$$

2.3 Electronic Energy states of SO_2

Unlike the case of diatomic molecule, the components of angular momentum in the non linear triatomic molecule do not commute with the electronic hamiltonian H_{el}. Therefore, the electronic energy level classification for the diatomic molecule is no longer applicable to the non linear triatomic molecules. However, the symmetric operators do commute with the electronic hamiltonian H_{el}, allowing for the classification of the electronic energy level to be based on the behavior of electronic wave function on application of these symmetric operators. The electronic states of SO_2 may then be named by their orbital symmetry A_1, A_2, B_1, B_2 in the usual nomenclature of the C_{2v} group to which SO_2 belongs. Moreover, if

we ignore the spin orbit interaction, the total electronic spin angular momentum operator S^2 commute with the electronic hamiltonian H_{el}. So for nonlinear polyatomic molecules the electronic energy level classification is carried out according to the behavior of wavefunction with respect to symmetry operator and the spin quantum number of the state. If S = 0, then the electronic state is said to be singlet state and if S = 1, then the electronic state is said to be the triplet state. The multiplicity is usually written on the left superscript like $^1A_1$, $^1B_1$, $^3B_1$, $^3A_2$. For SO_2, besides the ground electronic state $^1A_1$, two other singlet electronic states $^1B_1$ and $^1A_2$ and one triplet state $^3B_1$ were experimentally detected and extensively studied. However the presence of other triplet electronic states such as $^3B_2$ and $^3A_2$ were predicted by indirect evidences

2.4 Electronic and vibronic selection rule.

Electronic transitions mostly involve interaction between the molecules and the electric component of the electromagnetic radiation, hence, on first order approximation the selection rules may be considered as electron dipole selection rules [17]. The electronic transition intensity is proportional to $|M_e|^2$, the square of the electronic transition moment M_e .

$$M_e = \langle \psi_e' | \mu | \psi_e'' \rangle \qquad (2.4.1)$$

Where ψ_e' and ψ_e'' are the wave functions of upper and lower electronic states respectively and μ is the dipole moment operator. For an allowed electronic transition $| M_e | \neq 0$ and the symmetry requirements for M_e to have non-zero value is

$$\Gamma(\psi_e') \times \Gamma(\mu) \times \Gamma(\psi_e'') = \text{Totally symmetric} \qquad (2.4.2)$$

This is for transitions between two non degenerate electronic states. For the transition between two degenerate electronic states the above equation becomes

$$\Gamma(\psi_e') \times \Gamma(\mu) \times \Gamma(\psi_e'') \supset \text{Totally symmetric.} \qquad (2.4.3)$$

where the symbol $\supset$ is to emphasize that at least one of these two states involved in transition should be degenerate.

The components of M_e along the Cartesian axes are given by the following three expressions

$$M_{ex} = \langle \psi_e' | \mu_x | \psi_e'' \rangle$$

$$M_{ey} = \langle \psi_e' | \mu_y | \psi_e'' \rangle \qquad (2.4.4)$$

$$M_{ey} = \langle \psi_e' | \mu_y | \psi_e'' \rangle$$

Since $|M|^2 = |M_x|^2 + |M_y|^2 + |M_z|^2$ the electronic transition is allowed if any of the M_{ex}, M_{ey}, M_{ez} is non zero. The symmetric condition for any of the M_{ex}, M_{ey}, M_{ez} to be non zero, in order to allow transition between two non degenerate states is

$$\Gamma(\psi_e') \times \Gamma(T_x) \times \Gamma(\psi_e'') = \text{Totally symmetric}$$

$$\Gamma(\psi_e') \times \Gamma(T_y) \times \Gamma(\psi_e'') = \text{Totally symmetric} \qquad (2.4.5)$$

$$\Gamma(\psi_e') \times \Gamma(T_z) \times \Gamma(\psi_e'') = \text{Totally symmetric.}$$

(If a degenerate state is involved = is replaced by $\supset$)

From table 2.2 it is clear that if the product of two symmetry species is totally symmetric those species must be the same. Therefore we can write the above set of equations as

$$\Gamma(\psi_e') \times \Gamma(\psi_e'') = \Gamma(T_x) \text{ and / or } \Gamma(T_y) \text{ and / or } \Gamma(T_z) \qquad (2.4.6)$$

(If a degenerate state is involved = is replaced by $\supset$)

This is the general selection rule obtained with first order approximation for the transition between two electronic states.

If vibrations are excited in either the lower or the upper electronic state or both the vibronic transition moment M_{ev} corresponding to the electronic transition moment is given by

$$M_{ev} = \langle \psi_{ev}' \mid \mu \mid \psi_{ev}'' \rangle \qquad (2.4.7)$$

Where ψ_{ev}' and ψ_{ev}'' are the vibronic wave functions of upper and lower states respectively. Following the same argument for the electronic transition the selection rule for the vibronic transition becomes

$$\Gamma(\psi_{ev}') \times \Gamma(\psi_{ev}'') = \Gamma(T_x) \text{ and / or } \Gamma(T_y) \text{ and / or } \Gamma(T_z) \qquad (2.4.8)$$

Since $\Gamma(\psi ev) = \Gamma(\psi_e) \times \Gamma(\psi_v)$ equation 2.4.8 can be written as

$$\Gamma(\psi_e') \times \Gamma(\psi_v') \times \Gamma(\psi_e'') \times \Gamma(\psi_v'') = \Gamma(T_x) \text{ and / or } \Gamma(T_y) \text{ and / or } \Gamma(T_z) \qquad (2.4.9)$$

2.5 Normal modes of vibration of SO_2 and group vibration

A nonlinear molecule with N atoms has 3N - 6 vibrational motions or in other words 3N - 6 vibrational degrees of freedom. The number of vibrational degrees of freedom gives the number of fundamental vibrational frequencies of molecules or, in other words, the number of different normal modes of vibration. The normal modes of vibration of a molecule can be computed through the small oscillation formalism of classical mechanics [19]

The kinetic energy of the vibrating molecule is given by

$$2T = \sum_{\alpha=1}^{N} m_\alpha \left[\left(\frac{d\Delta x_\alpha}{dt} \right)^2 + \left(\frac{d\Delta y_\alpha}{dt} \right)^2 + \left(\frac{d\Delta z_\alpha}{dt} \right)^2 \right] \qquad (2.5.1)$$

Where $\Delta x_\alpha, \Delta y_\alpha, \Delta z_\alpha$ are the displacement of the αth atom from the equilibrium position and m_α is mass of the αth atom. It is very convenient to replace the coordinates $\Delta x_\alpha, \Delta y_\alpha, \Delta z_\alpha$ by new set of coordinates $q_1, q_2 \ldots\ldots\ldots\ldots\ldots q_{3N}$ defined as follows.

$$q_1 = \sqrt{m_1}\Delta x_1;\ q_2 = \sqrt{m_1}\Delta y_1;\ q_3 = \sqrt{m_1}\Delta z_1;\ q_4 = \sqrt{m_2}\Delta x_2 \qquad (2.5.2)$$

These coordinates are known as mass weighted Cartesians displacement coordinates. In terms of time derivative of these coordinates the kinetic energy can be written as

$$2T = \sum_{i=1}^{N} \dot{q}_i^2 \tag{2.5.3}$$

The potential energy V will be some function of displacements and therefore it is the function of the q's. For small values of displacements, the potential energy V may be expressed as the power series of the displacement q_i.

$$2V = 2V_0 + 2\sum_{i=1}^{3N} \left(\frac{\partial V}{\partial q_i}\right)_0 q_i + \sum_{i,j=1}^{3N} \left(\frac{\partial^2 V}{\partial q_i q_j}\right) q_i\, q_j + \text{higher terms} \tag{2.5.4}$$

$$2V = 2V_0 + 2\sum_{i=1}^{3N} f_i\, q_i + \sum_{i,j=1}^{3N} f_{ij}\, q_i\, q_j + \text{higher terms} \tag{2.5.5}$$

By choosing the zero of energy so that the energy of the equilibrium configuration is zero, V_0 may be eliminated. Furthermore,

when all q's are zero, the atoms are all in their equilibrium position so that the energy must be minimum for $q_i = 0$; $i = 1,2,3$ ..... Therefore

$$\left(\frac{\partial V}{\partial q_i}\right)_0 = f_i = 0 \qquad i = 0,1,2,.....3N \tag{2.5.6}$$

For sufficiently small amplitudes of vibration, the higher terms can be neglected so that

$$V = \sum_{i,j=1}^{3N} f_{ij}\, q_i\, q_j \tag{2.5.7}$$

in which f_{ij} are constants given by

$$f_{ij} = \left(\frac{\partial^2 V}{\partial q_i\, q_j}\right)_0 \tag{2.5.8}$$

with $f_{ij} = f_{ji}$. Newton's equations of motion can be written in the form

$$\frac{d}{dt}\left(\frac{\partial T}{\partial q_i}\right) + \frac{\partial V}{\partial q_i} = 0 \qquad i= 1,2,3, ... 3N. \tag{2.5.9}$$

Since T is the function of velocity only and V is the function of coordinates only, the substitution of the expressions of T and V given above yields the equations

$$\ddot{q}_j = \sum_{i=1}^{3N} f_{ij}\, q_i = 0 \qquad j = 1,2,3, \ldots\ldots\ldots 3N \qquad (2.5.10)$$

This is a set of 3N simultaneous second order linear differential equations. One possible solution is

$$q_i = A_i \cos\left(\sqrt{\lambda}\, t + \varphi\right) \qquad (2.5.11)$$

Where A_i, λ and φ are properly chosen constants. If these expressions are substituted in the differential equation, a set of algebraic equations results

$$\sum_{i=1}^{3N} (f_{ij} - \delta_{ij}\lambda)\, A_i = 0 \qquad j = 1,2,3\ldots\ldots\ldots 3N \qquad (2.5.12)$$

in which δij is the Kronocker delta function. Equation 2.5.12 is a set of simultaneous homogeneous linear algebraic equations in 3N unknown amplitudes A_i

Only for special values of λ, equation 2.5.11 will have non vanishing solutions; for all other values of λ the solution is trivial one $A_i = 0$, i=1,2,3, ... 3N corresponding to no vibration. The special values of λ are those which satisfy the secular equation.

$$\begin{vmatrix} f_{11}-\lambda & f_{12} & \cdots\cdots & f_{1,3N} \\ f_{21} & f_{22}-\lambda & \cdots\cdots & f_{2,3N} \\ \cdot & \cdot & \cdot & \cdot \\ \cdot & \cdot & \cdot & \cdot \\ \cdot & \cdot & \cdot & \cdot \\ f_{3N,1} & f_{3N,2} & \cdots\cdots & f_{3N,3N}-\lambda \end{vmatrix} = 0 \qquad (2.5.13)$$

The elements of this determinants are the coefficients of unknown amplitudes A_i in the set of equation 2.5.12. When a fixed value of λ say λ_k is chosen so as to cause the determinant to vanish, the coefficient of the unknown A_i in equation 2.5.12 becomes fixed and then it is possible to obtain a solution A_{ik}, for which the additional subscript k will be used to indicate the correspondence with the particular value of λ_k. Such system of equations does not determine A_{ik} uniquely, but gives only their roots. A convenient and unique mathematical solution may be designated by the quantities l_{ik} which are defined in terms of an arbitrary solution, A_{ik}' by the formula

$$l_{ik} = \frac{A_{ik}'}{\left[\sum_i (A_{ik}')^2\right]^{\frac{1}{2}}} \qquad (2.5.14)$$

Note that these amplitudes are normalized in the sense that

$$\sum_i l_{ik}^2 = 1 \qquad (2.5.15)$$

The solution of the actual physical problem then can be obtained by putting

$$A_{ik} = K_k \, l_{ik} \qquad (2.5.16)$$

where K_k are constants determined by the initial values of the coordinates q_i and velocity $\dot{q}$.

It can be shown that six of the roots are zero so that the equation reduces to one with the 3N - 6 degree. There are thus 3N - 6 non zero roots of the secular equation. It is evident that each atom is oscillating about its equilibrium position with a simple harmonic motion of amplitude $A_{ik} = K_k \, l_{ik}$ and frequency $\nu_k = \frac{\sqrt{\lambda_k}}{2\pi}$ where λ is identified as the square of the angular frequency for the k th degree of freedom. In the case of SO_2 it has three atoms and hence the secular equation becomes.

$$\begin{vmatrix} f_{11} - \lambda & f_{12} & \cdots\cdots & f_{19} \\ f_{21} & f_{22} - \lambda & \cdots\cdots & f_{29} \\ \cdot & \cdot & \cdot & \cdot \\ \cdot & \cdot & \cdot & \cdot \\ \cdot & \cdot & \cdot & \cdot \\ f_{391} & f_{92} & \cdots\cdots & f_{99} - \lambda \end{vmatrix} = 0$$

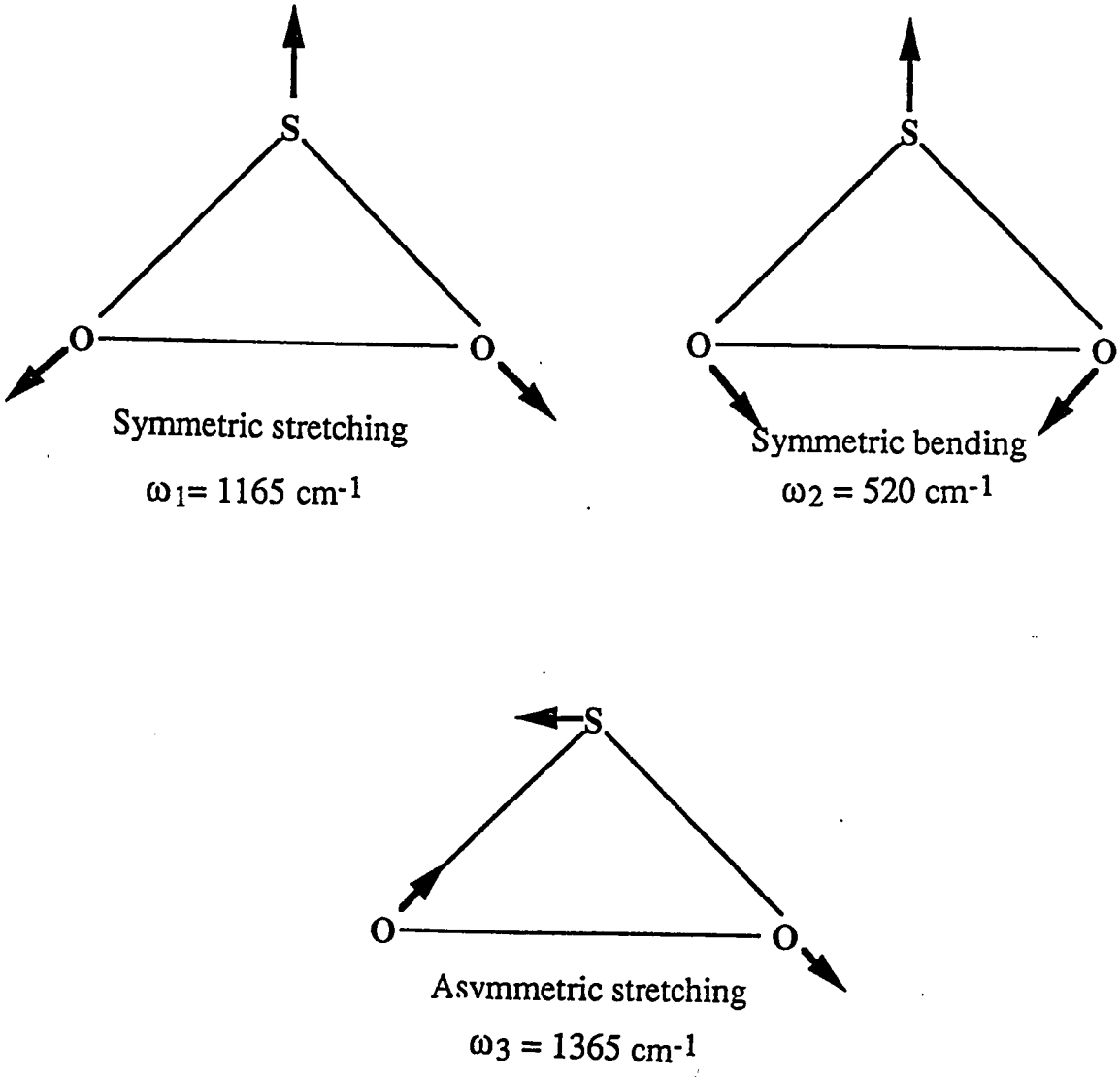

figure: 2.3 Three normal modes of vibration of SO2

This equation has nine roots, of which 6 of them are zero, and therefore there are 3 non zero roots. As mentioned before, three roots of the secular equation can be identified as the square of the angular frequency of the normal modes of vibration. Hence SO_2, has three normal modes of vibrations. (1) Symmetric stretch (2) Symmetric bend and (3) antisymmetric stretch, where the symmetric stretch frequency of the ground state has been determined by Raman techniques to be 1165 cm^{-1}, that of symmetric bend to be 520 cm^{-1} and that of asymmetric stretch to be 1365 cm^{-1}. The three normal modes of vibrations and their frequencies are shown in figure 2.3.

2.6 Energy levels of the Vibrating Molecule

In order to carry out the quantum mechanical treatment of molecular vibrations, it is necessary to introduce a new set of coordinates Q_k, k =1,2,3..... 3N called normal coordinates. There is one normal coordinate associated with each normal mode of vibration. The normal coordinates are defined in terms of the mass weighted coordinate displacement coordinates q_i by the linear equation.

$$Q_k = \sum_{i=1}^{3N} l_{ki}\, q_i \qquad k = 1,2,3,..... 3N \qquad (2.6.1)$$

in which the coefficients l_{ki} have been chosen so that in terms of new coordinates the kinetic and potential energy has the forms.

$$2T = \sum_{k=1}^{3N-6} \dot{Q}_k^2 \qquad (2.6.2)$$

$$2V = \sum_{k=1}^{3N-6} \lambda_k Q_k^2 \qquad (2.6.3)$$

The vibrational wave equation then will have the form

$$-\frac{h^2}{8\pi^2} \sum_{k=1}^{3N-6} \left(\frac{\partial^2 \psi_v}{\partial Q_k^2}\right) + \frac{1}{2} \sum_{k=1}^{3N-6} \lambda_k Q_k \psi_v = E_v \psi_v \qquad (2.6.4)$$

Where E_v is the vibrational energy and Ψ_v is the vibrational wave function.

The advantage of using the normal coordinates will now be evident, since the wave equation 2.6.4. in this form is separable into 3N - 6 equations, one for each normal coordinate. Let

$$E_v = E(1) + E(2) + \ldots\ldots\ldots\ldots E(3N\text{-}6) \qquad (2.6.5)$$

$$\psi_v = \psi(Q_1)\, \psi(Q_2) \ldots\ldots\ldots\ldots\psi(Q_{3N\text{-}6}) \qquad (2.6.6)$$

Then it will be seen that the wave equation 2.6.4 is satisfied if the wave functions and the energies satisfy the equations of the type

$$-\frac{h^2}{8\pi^2}\left(\frac{d^2\psi(Q_k)}{dQ_k^2}\right)+\frac{1}{2}\lambda_{lk}\,Q_k\,\psi(Q_k) = E(k)\,\psi(Q_k) \qquad (2.6.7)$$

Each of the equation is a total differential equation in one variable Q_k. The above equation is the well-known wave equation for the linear harmonic oscillator, expressed in terms of normal coordinates Q_k, instead of usual linear coordinates x. The solution ψ_v of the vibrational problem is therefore expressible as a product of harmonic oscillator wave function $\psi(Q_k)$, one for each normal coordinates, while the total vibrational energy E_v is the sum of vibrational energies of the 3N-6 harmonic oscillators.

The energy levels of the linear harmonic oscillator is given by the expression

$$E = (n+\tfrac{1}{2})\,h\nu \qquad n = 0, 1, 2, \ldots\ldots \qquad (2.6.8)$$

where n is the quantum number which can take on any positive integral value including zero, while ν is the classical frequency of the system and h is the plank's constant. Consequently the vibrational energy of the molecule with several classical frequencies ν_k is given by

$$E = \sum_{i=1}^{3N-6} (n_i + \tfrac{1}{2})\, h\nu_i \qquad (2.6.9)$$

or writing in another form

$$G(\nu) = \sum_{i=1}^{3N-6} (n_i + \tfrac{1}{2})\, \omega_i \qquad (2.6.10)$$

where $G(\nu) = \frac{E}{hc}$ is of the dimension of wavenumber. Every normal coordinate Q_k has associated with it a quantum number n_k and normal frequency ν_k, These latter frequency being the classical normal frequencies of vibration.

The lowest vibrational level is called ground level, for which all the quantum numbers are zero. The energy of this level is called zero point energy of the molecule and is equal to $\frac{1}{2} h \sum_{k=1}^{3N-6} \nu_k$. The energy levels for which all the quantum numbers are zero except one for which the value is unity are called the fundamental levels. When only one normal vibration is excited, i.e. when only one ν_k is different from zero, but the quantum number is greater than one, the corresponding energy levels are called overtones. When two or more quantum numbers have non zero values, the resulting values are known as combination levels.

Table 2.3 Anharmonic constants of SO_2 in the ground State

Vibrational constants	Values from Reference 19
ω1	1167.84
ω2	522.21
ω3	1382.18
x11	-3.655
x22	-0.374
x33	-5.36
x12	-3.129
x13	-14.277
x23	-4.122
y111	-0.0061
y222	-0.0014
y333	-0.031
y112	-0.0001
y113	-0.1574
y122	-0.0063
y123	-0.0509
y133	0.255
y223	0.0214
y233	-0.008

As energy is increased, the energy level diagram of the polyatomic molecule becomes increasingly and rapidly complicated. This is due to the anharmonicity that arises due to the higher terms in the power series expansion of the potential energy in equation 2.5.4 . So far it has been assumed that only the quadratic term in the potential energy is to be considered. In actual practice the higher terms are ofcourse not zero and may have to be taken into account for certain purposes. The most obvious effect of the higher or anharmonic term is upon the position of overtones and combination levels.The harmonic oscillator has equally spaced overtone levels so that the vibrational energy level of a molecule with 3N -6 fundamental frequencies ν_k would be with neglect of the anharmonic terms and is given by the equation 2.6.8.

In the presence of anharmonicities [20] equation 2.6.10 is written as

$$G(\nu_1\,\nu_2\,\nu_3) = \sum_i \omega_i\,(n_i + \frac{1}{2}) + \sum_{i<j} X_{ij}\,(n_i + \frac{1}{2})\,(n_j + \frac{1}{2}) + \sum_{i<j<k} Y_{ijk}\,(n_i + \frac{1}{2})(n_j + \frac{1}{2})(n_k + \frac{1}{2}) \qquad (2.6.11)$$

where X_{ij}, Y_{ijk} are the anharmonic terms arises due to the higher terms in the power series expansion of the potential energy in equation 2.5.4. The

various anharmonic terms [19] of SO_2 in the ground state are listed in table 2.3.

2.7 Vibrational progressions and Franck - Condon Treatment for SO_2

Vibrational transitions accompanying the electronic transitions are referred to as vibronic transitions. Vibronic transitions may be divided into progressions. A progression involves series of vibronic transitions with a common upper or lower level. In an absorption spectrum a molecule is excited from a common lower level to a series of vibrational levels in the upper electronic state. In the emission spectrum, a single excited upper vibronic level decays to a series of vibrational levels in the lower electronic state.

A vibrational level can either be fundamental level or overtone level or combination level. In a single vibronic progression there could be some sub progressions of the individual modes of vibrations. For example in the case of SO_2, three types of sub progressions can be present. i.e. ν_1 ν_2 and ν_3 progressions. ν_1 progression for example is, a set of progressions originating from same vibrational levels (upper or lower) to the vibrational levels (lower or upper), whose quantum number associated with the ν_1 mode of vibration changes from 0 to n, while the quantum

numbers associated with other two modes of vibrations are fixed to a certain value.

Franck - Condon principle provides the basic guide for understanding the intensities of the vibrational bands [21]. A classical formulation of the Franck - Condon principle goes as follows. "an electronic transition takes place so rapidly that a vibrating molecule does not change its internuclear distance appreciably during the transition". Figure 2.4 shows three possibilities. In (a) we show the upper electronic state having the same equilibrium internuclear distance as the lower. Now the Franck-Condon principle suggests that a transition occurs vertically on this diagram, since the internuclear distance does not change, and if we consider the molecule to be in the ground state both electronically and vibrationally, then the most probable transition is that indicated by the vertical line in figure 2.4. Thus the strongest spectral line will be (0,0). However the quantum theory only says that the probability of finding the oscillating atom is greatest at the equilibrium distance in the $v = 0$ state. It allows some, although small, chance of atom being near the extremities of its vibrational motion. Hence there is some chance of transition starting from the ends of the $v'' = 0$ state and finishing in the $v' = 1, 2$, etc., states. The (0, 1), (0,2) etc. lines diminish rapidly in intensity, as shown at the foot of figure 2.4 a.

In figure 2.4 b we show the case where the excited electronic state has a slightly greater internuclear separation than the ground state.

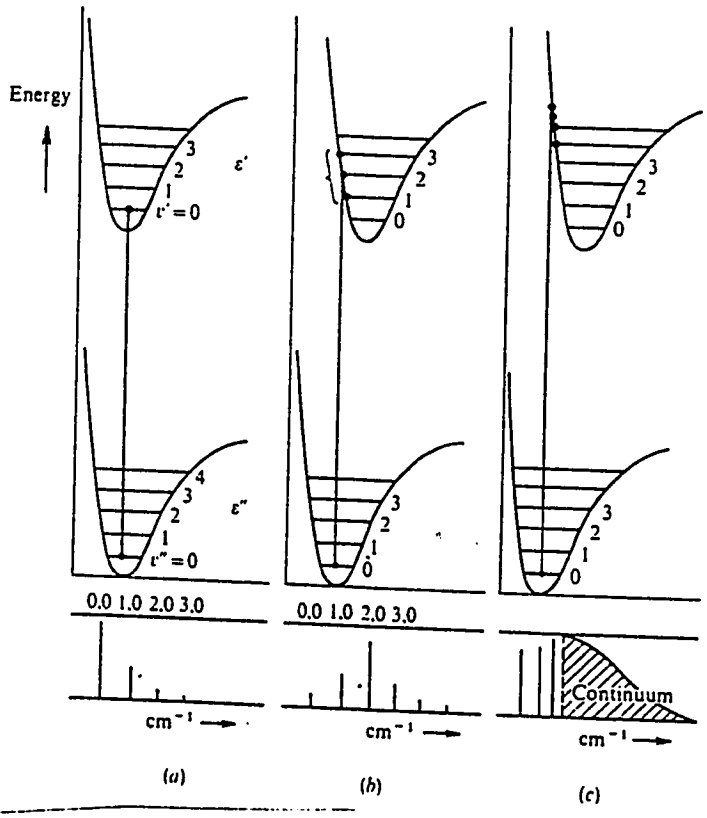

Figure : 2.4 The operation of Frank - Condon principle for (a) inter nuclear distances equal in upper and lower states., (b) upper-state inter nuclear distance a little greater than that in the lower state, and (c) upper-state distance considerably greater.

Now the vertical transition from $\nu'' = 0$ level will most likely to occur into the upper vibrational state $\nu' = 2$, transition to lower and higher ν' states being less likely; in general the upper state most probably reached will depend on the difference between the equilibrium separations in the lower and upper states. In figure 2.4 c the upper state separation is drawn as considerably greater than that in the lower state and we see that, firstly , the vibrational level to which the transition take place has a high ν' value. Further transitions can now occur to a state where the excited molecules has the energy in excess of its own dissociation energy. From such states the molecules will dissociate with out any vibrations and, since the atoms which are formed may take up any value of kinetic energy, the transitions are not quantized and a continuum results. This is shown at the foot of the figure.

First quantum mechanical qualitative treatment of Franck - Condon principle for SO_2 was carried out by Coon et al [22]. Using the Born - Oppenheimer approximation, the transition moment for the transition between the n th vibrational level in the lower electronic state l and the m th vibrational level of the upper electronic state u can be written as

$$M_{um \rightarrow ln} = \langle \psi_{um}(Q) \mid M_{ul}(Q) \mid \psi_{ln}(Q) \rangle_Q \qquad (2.7.1)$$

where

$$M_{ul}(Q) = \langle \psi_l(x,Q) \mid \mu(x) \mid \psi_u(x,Q) \rangle \qquad (2.7.2)$$

Here x and Q represent the electronic and nuclear coordinates respectively. $\psi(x,Q)$ and $\psi(Q)$ represent electronic and vibrational wave function respectively, where $\mu(x)$ is the electronic dipole operator. The subscript in the matrix element bracket indicate the integration over these coordinates. M_{ul} is the electronic transition moment for the nuclei fixed in the configuration Q. It may be expanded as the power series in the normal coordinates Q_r about the equilibrium position of one of the states, perhaps the ground state.

$$M_{ul} = M_{ul}(0) + \sum_{r} \left(\frac{\partial M}{\partial Q_r}\right) Q_r + \frac{1}{2} \sum_{r,s}^{?} \left(\frac{\partial^2 M}{\partial Q_r \partial Q_s}\right) Q_r Q_s + \ldots\ldots\ldots \qquad (2.7.3)$$

Frequently it may be assumed that $M_{ul}(Q)$ varies only slightly over the region of overlap of the vibrational wave function of interest, and that $M_{ul}(Q)$ may be replaced by $M_{ul}(0)$. In this case the transition moment of equation 2.7.3 becomes

$$M_{um \rightarrow ln} = M_{ul}(0) \langle \psi_{um}(Q) | \psi_{ln}(Q) \rangle \qquad (2.7.4)$$

and the intensity of the band is proportional to the square of this quantity. For absorption this quantity may be written as

$$I^{a}_{ln \rightarrow um} = K_a \, \bar{\nu}_{ln,um} \left| M_{um,ln} \right|^2$$

$$= K_a \bar{\nu}_{ln,um} \, |M_{ul}(0)|^2 \, |\langle \psi_{ln} | \psi_{um} \rangle|^2 \qquad (2.7.5)$$

Where $$K_a = \frac{8\pi^3 N}{3000\, hc\, (\ln 10)} \qquad (2.7.6)$$

Where N is the Avogadro number and $\bar{\nu}$ is the wavenumber. The frequency usually varies only very slightly over the electronic band, so the relative intensity is mainly determined by the term $|\langle \psi_{ln} | \psi_{um} \rangle|^2$, which is called the Franck - Condon factor, which is the measure of the degree to which the two vibrational wave functions overlap. For emission the intensity of the vibronic band is measured by the number of quanta emitted per second in that band per molecule in the initial state. This is given by

$$I^e_{um \to ln} = K_e \bar{\nu}^3_{um,ln} \, |M_{um,ln}|^2$$

$$= K_e \bar{\nu}^3_{um,ln} \, |M_{ul}(0)|^2 \, |\langle \psi_{um} | \psi_{ln} \rangle|^2 \qquad (2.7.7)$$

Where $$K_e = \frac{64\,\pi^4}{3h} . \qquad (2.7.8)$$

Vikesland and Strickler [13] applied the method of Coon et al to their data on absorption intensity. This was done as follows.

(1) The vibrational wave functions are assumed to be expressible as the product of the harmonic oscillator wave functions each of which refers to as a normal coordinate.

(2) The normal coordinates of the excited state are assumed to be parallel to those of the ground state, i.e. the origin is displaced but the coordinate system is not rotated. This reduces the Franck - Condon factors of equation 2.7.5 and equation 2.7.7 to the product of the Franck - Condon Factors for the individual modes.

(3) The displacement of the origin along the symmetric normal coordinates Q_1 and Q_2 are varied until a good fit is obtained to the relative intensities of the vibrational band.

An excellent fit to the observed intensities of the strong bands in the clearly assignable region of the absorption spectrum was obtained using displacements very similar to that of Coon et al [22]. However, when the same displacements were used to calculate the phosphorescence spectrum, the calculated intensities, disagreed dramatically with the observed system. It was possible to fit the emission spectrum, only using a larger set of displacement. Since the displacement define the equilibrium position of the excited state and this must be same for either spectrum. The simple Franck - Condon treatment outlined above is clearly inadequate. This failure was due to the inadequacy of the assumption that only zero order term of equation 2.7.3 was important. If we retain the next term as well, the transition moment becomes.

$$M_{ln,um} = \left\langle \psi_{ln} \middle| M_{ul}(0) + \sum_r \left(\frac{\partial M_{ul}}{\partial Q_r}\right)_0 Q_r \middle| \psi_{um} \right\rangle \qquad (2.7.9)$$

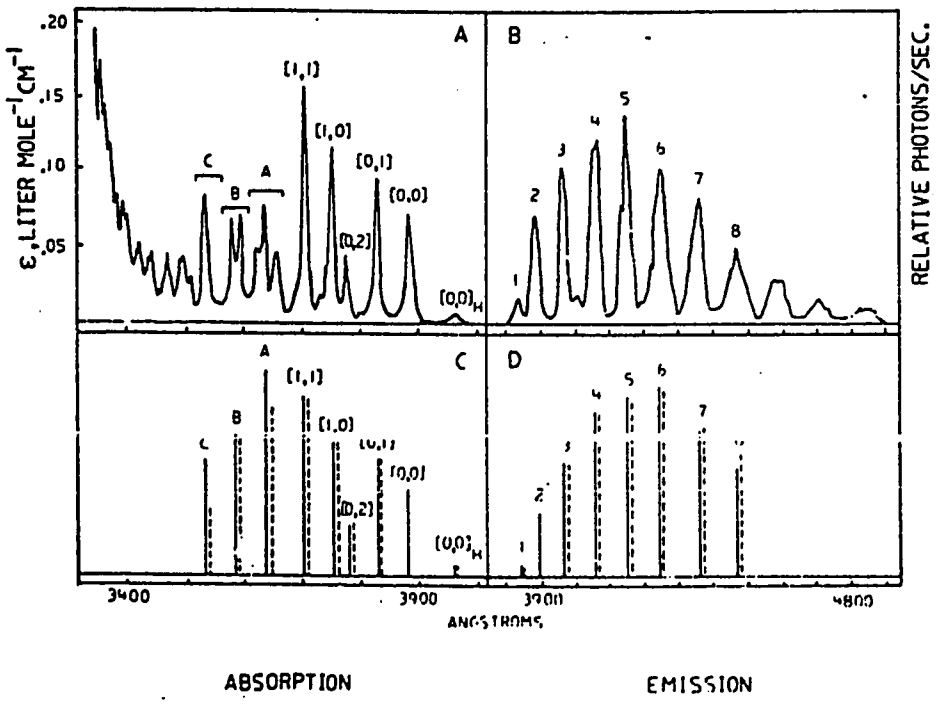

Figure : 2.5 The $^3B_1$ - $^1A_1$ transition of SO_2 gas
(A) Absorption spectrum (B) Emision spectrum
(C) Relative intensities in absorption (D) Relative intensities in emision. Solid line - observed. dashed line - calculated

Since Q_2 requires significantly larger displacement to fit the emission spectrum, we assume that the transition moment is influenced only by this bending vibration. The formula for intensities then contain a Franck - Condon factor for the Q_1 mode and a modified intensity factor for Q_2 mode. We can write the analog of equation 2.7.5 as

$$I^{a}_{ln\rightarrow um} = K_a \bar{\nu}_{ln,um} \left| M_{ul}(0) \right|^2 \left| \langle \psi_{um_1}(Q_1) | \psi_{ln_1}(Q_1) \rangle \right|^2 \times \left| \langle \psi_{um_2}(Q_2) | 1 + \rho Q_2 | \psi_{ln_2}(Q_2) \rangle \right|^2 \qquad (2.7.10)$$

where $\rho = \frac{1}{M_{ul}(0)} \left(\frac{\partial M_{ul}}{\partial Q_2} \right)_0$ is the ratio of the derivatives of the transition moment to its value at the equilibrium position of the ground state. The corresponding equation for emission is

$$I^{e}_{um\rightarrow ln} = K_e \bar{\nu}^3_{um,ln} \left| M_{ul}(0) \right|^2 \left| \langle \psi_{um_1}(Q_1) | \psi_{ln_1}(Q_1) \rangle \right|^2 \times \left| \langle \psi_{um_2}(Q_2) | 1 + \rho Q_2 | \psi_{ln_2}(Q_2) \rangle \right|^2 \qquad (2.7.11)$$

The value of ρ was varied until a fit to both spectra was obtained using equation 2.7.9 and equation 2.7.10.

Figure 2.5 shows the calculated and observed relative intensities of both emission and absorption. The solid lines indicate the observed intensities and dashed line indicate the calculated intensities.

Although it is not possible to measure the relative intensities of the single vibronic bands in the 3680 - 3510 Å region of absorption spectrum, it is possible to separate the three band groups. These regions are labeled A, B and C in the figure. Region A and C have observed intensities which are significantly greater than the summation of the calculated intensities of the appropriate vibronic bands. In the case of region C this difference is of about a factor two. This difference can not be reasonably explained in terms of inaccuracy in either the measurement of the spectrum or calculation of intensities. Hence these results may indicate the presence of other triplet electronic transitions.

2.8 Effect of SO_2 concentration

In supersonic jet, the concentration of SO_2 can be adjusted by premixing SO_2 and carrier gas (Ar, He etc.) to a desired ratio with the help of a needle valve, and also by changing the nozzle to laser distance. Recently Al- Adel et al [23] reported a strong dependence of SO_2 vibrational and rotational temperature on SO_2 concentration. The effect of concentration on the rotational temperature is illustrated in figure 2.6 a by a series of excitation scans of 30552 cm^{-1} band, in which we can notice as the concentration of SO_2 decreases, the width of the vibrational band is narrowed down and the individual vibronic bands are separated from each

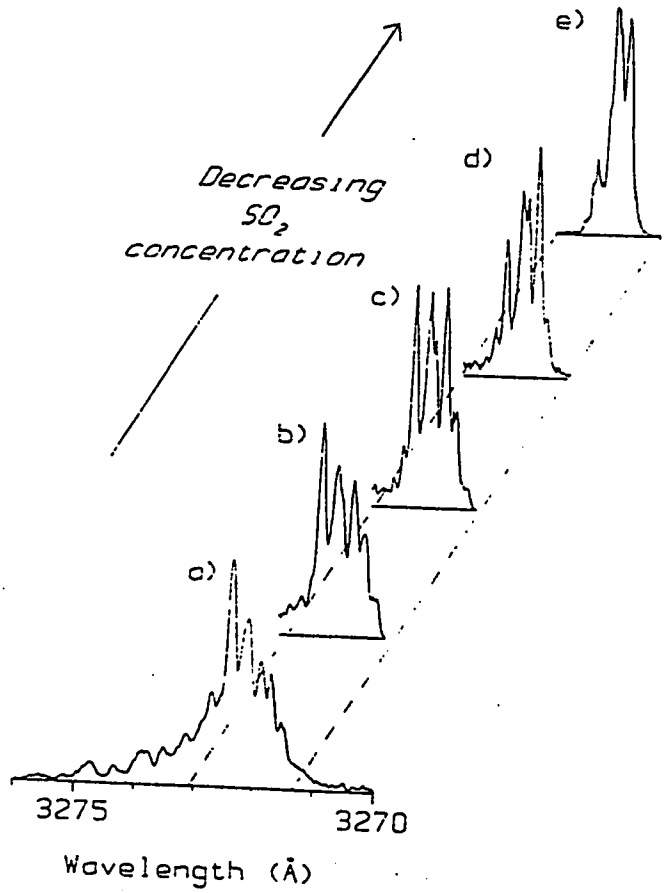

Figure : 2.6 a Effect of SO_2 concentration on the rotational contour.

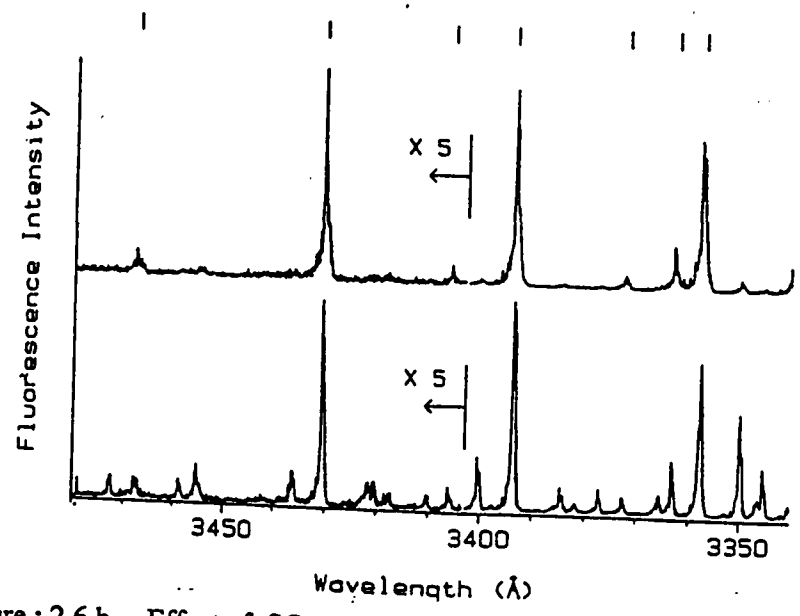

Figure : 2.6 b Effect of SO_2 concentration on the vibrational bands

other. Thus it is evident that the rotational temperature (T_{rot}) of SO_2 is lowest for the low SO_2 concentration.

Figure 2.6 b is the fluorescence excitation spectra of SO_2, in which the upper spectrum is for high concentration and the lower one is for the moderate concentration. Although the bands are broad in the upper scan, the vibrations are well resolved and some of the vibrational bands have disappeared. So we can assign the bands that disappeared at higher concentration to be the hot bands that originate from the higher vibrational states. Thus it is clear that the high concentration of SO_2 is much more effective at vibrational cooling of SO_2. Therefore there is a inverse relationship between the vibrational and rotational temperatures with respect to concentration. The concentration dependence observed is an evidence that SO_2 vibrations are more effectively relaxed by collision with other SO_2 molecules than the molecules of the carrier gas, while the reverse is true for rotation.

2.9 Various Couplings in the First Allowed Band of SO_2

Hamada and Merrer [4] confirmed that the first allowed absorption band is due to $^1A_2 \leftarrow\!\!- \ ^1A_1$ transition. This transition is electronically forbidden but can be made allowed through the vibronic coupling with $^1B_1$ state, if an odd number of quanta in asymmetric stretching vibration is excited in $^1A_2$ state. The vibronic coupling has two

aspects [24]; the Herzberg- Teller coupling caused by the dependence of the electronic transition moment on the nuclear position and the Born-Oppenheimer coupling due to the breakdown of the Born - Oppenheimer approximation [25]. The ratio of the coupling matrix element is of the order of $M^{BO}/M^{HT} = h\omega/(2\pi\Delta E)$, where $(h\omega/2\pi)$ is the vibrational energy and ΔE is the energy seperation between these two coupled states. At longer wavelengths, well below the origin of $^1B_1$ state, where $\Delta E >> h\omega/2\pi$ the Herzberg - Teller coupling is dominant where as above 32000 cm^{-1} the Born - Opperheimer coupling will be dominant.

Through another work Hamada and Merrer [5] have given a comprehensive treatment of the first allowed transition in SO_2. The relative intensities of the bands in this system were calculated by using the known electronic transitions induced by the Herzberg - Teller coupling, and they concluded that this pattern could only be explained if a second electronic transition from which $^1A_2 \rightarrow {}^1A_1$ transition can borrow intensity is also present. They pointed out that there are two electronic transition in the first allowed absorption band of SO_2: one is the forbidden $^1A_2 \rightarrow {}^1A_1$ transition which is made allowed through asymmetric stretch ν_3. The other transitions $^1B_1 \rightarrow {}^1A_1$ transition appears only as a back ground of weak absorption line beneath the stronger $^1A_2 \rightarrow {}^1A_1$ transition, which accounts for all analyzable bands in the system.

The $^1B_1$ state is strongly Renner coupled to many ground state levels. The dense manifold of the ground state level interacts with the

sparse manifold of the $^1B_1$ levels through Renner coupling which further interacts with the slightly denser $^1A_2$ level through Born- Oppenheimer coupling. The hybrid level resembles the vibrational structure of $^1A_2$ level. Brand et al [12] observed strong Zeeman effect in the $^1A_2 \rightarrow {}^1A_1$ band system and calculated that these couplings alone can not explain the strong Zeeman effect observed. They pointed out that there must be a singlet triplet coupling through the spin orbit interaction.

The time resolved study of Brus and Mc Donald [8,9] revealed that the fluorescence decay of SO_2 fluorescence was a doubly exponential decay and they fitted their intensity results to the expression

$$I(t) = I_S \exp(-t/\tau_S) + I_L \exp(-t/\tau_S) \qquad (2.9.1)$$

where I_S, τ_S and I_L,τ_L are the intensities and the lifetimes of the short and the long components respectively. Brus and McDonald believed that the long lived fluorescence is from $^1A_2$ and the short lived fluorescence is from $^1B_1$. Later Caton and Gangadharan [10] pointed out that the short lived and long lived fluorescence are from the electronic state of same symmetry. They assigned that the fast fluorescence to be from $^1B_1$, which is strongly Renner coupled to the ground state while the slow fluorescence is from the state which is weakly Renner coupled to the ground state. The short lived and the long lived fluorescence are designated as $^1B_1(S)$ and $^1B_1(L)$ respectively.

2.10 Production of singlet and triplet states and Emission of fluorescence and Phosphorescence .

There are two electronic states formed in the first allowed absorption:

$$^1A_1 + h\nu \xrightarrow{\text{Strong absorption}} {}^1A_2{}^n \qquad (2.10.1)$$

$$^1A_1 + h\nu \xrightarrow{\text{weak absorption}} {}^1B_1{}^n\,(L) \qquad (2.10.2)$$

The stronger absorption produces $^1A_2$ state, even though the transition is forbidden. It becomes allowed through Herzberg - Teller coupling with the $^1B_1$ state. However, this coupling occurs only through the odd vibrational levels of the symmetric stretch in $^1A_2$. Thus the superscript n on $^1A_2$ in equation 2.10.1 refers specifically to these vibrational levels (n = 1,3,5....). The weaker absorption produces vibrationally excited $^1B_1$ levels, though these do not necessarily have to be in the asymmetric stretch. This state is responsible for the long lived fluorescence and is designated as $^1B_1{}^n$ (L) in equation 2.10.2. This absorption occurs because of the coupling of $^1B_1{}^n$ (L) to the triplet manifold.

The short lived fluorescence has been shown by spectral analysis to arise from the $^1B_1$ state[10,26 -28]. Furthermore, the fluorescence quenching Stern- Volmer plots of Stockberger et al [29] showed upward deviation at high pressures indicating that the major emission could not arise from the state produced on absorption. Therefore the principal fate of the $^1A_2{}^n$ state at low pressures must be rapid internal conversion to $^1B_1{}^n$ (S) state, but we can expect weak fluorescence from the $^1A_2$ state also.

$$^1A_2{}^n \xrightarrow{\text{internal conversion}} {}^1B_1{}^n\,(S) \qquad (2.10.3)$$

The $^1B_1$ state formed in equation 2.10.3 is vibrationally excited. The superscript *n* may refer to excitation in any vibrational levels of the $^1B_1{}^n$ (S) state, unlike the case of $^1A_2{}^n$. The $^1B_1{}^n$ (S) state produced is not coupled to the triplet manifold. (or it would have formed directly on absorption) and is responsible for the short lived fluorescence.

At zero pressures the fluorescence quantum yield is 1.0, so the dominant removal process for the $^1B_1{}^n$ state must be fluorescence. Also we can expect fluorescence from the $^1A_2$ state.

$$^1A_2{}^n \longrightarrow {}^1A_1 + h\nu_f \qquad (2.10.4)$$

$$^1B_1{}^n\,(L) \longrightarrow {}^1A_1 + h\nu_f \qquad (2.10.5)$$

$$^1B_1{}^n\,(S) \longrightarrow {}^1A_1 + h\nu_f \qquad (2.10.6)$$

Phosphorescence from the $^3B_1$ state is also observed when absorption is into the first allowed band. Some of the absorption, specifically in the 3000 -3300Å region is directly to $^1B_1{}^n$ (L) which is coupled to the triplet manifold. Presumably this state can cross over to the $^3B_1$ state to produce phosphorescence at low pressures.

$$^1B_1{}^n\,(L) \xrightarrow{\text{intersystem crossing}} {}^3B_1{}^n \qquad (2.10.7)$$

$$^3B_1 \longrightarrow {}^1A_1 + h\nu_p \qquad (2.10.8)$$

At high pressures collissional processes take place. For the $^1A_2{}^n$ state, the data of Stockburger et al demonstrate that the collisional quenching does not give the $^1B_1$ state. Since the quenching coefficient is large, it seems that $^1A_2{}^n$ state is more likely to lead to vibrational deactivation than cross over to a forbidden electronic state ($^1A_1$ or any triplet states). So the major process is the vibrational deactivation.

$$^1A_2{}^n + M \longrightarrow {}^1A_2{}^0 + M \qquad (2.10.9)$$

$^1A_1{}^0$ state is no longer coupled to the $^1B_1$ state. It must have a very long life-time and it eventually decays to $^1A_1$ state after a long time

$$^1A_2{}^0 + M \longrightarrow {}^1A_1 + M \qquad (2.10.10)$$

The collisional quenching of $^1B_1{}^n(L)$ must produce $^3B_1$.

$$^1B_1{}^n(L) + M \longrightarrow M + {}^3B_1 \qquad (2.10.11)$$

The fractional fluorescence intensity f_s of short lived state, obtained for higher pressure is smaller than that obtained for the zero pressure limit at any excitation wavelength[1]. Hence collisional quenching of $^1B_1{}^n$ (S) state will produce $^1B_1{}^m$ (L) state.

$$^1B_1{}^n(S) + M \longrightarrow {}^1B_1{}^m(L) + M \qquad (2.10.12)$$

The final state $^1B_1{}^m(L)$ rather than $^1B_1{}^n(L)$ indicates, the new state has slightly different vibrational energy level. Also $^1B_1{}^m(L)$ state may not be strongly coupled to the triplet manifold as $^1B_1{}^n(L)$, because it represents smear of states. Thus equation 2.10.12 lengthens the fluorescence life time, but not necessarily to the same extent as direct absorption to $^1B_1{}^n(L)$ state.

As pressure is raised the fluorescence is red shifted. This indicates that some sort of vibrational deactivation, similar to equation 2.10.9 occur for both $^1B_1{}^n(L)$ and $^1B_1{}^n(S)$ as a result of collisional quenching.

$$^1B_1{}^n(S) + M \longrightarrow {}^1B_1{}^0 + M \qquad (2.10.13)$$

$$^1B_1{}^n(L) + M \longrightarrow {}^1B_1{}^0 + M \qquad (2.10.14)$$

$$^1B_1{}^0 + M \longrightarrow {}^1A_1 + M \qquad (2.10.15)$$

$^1B_1{}^0$ state, on further collision comes back to the $^1A_1$ as in equation 2.10.14.

No triplet states other than $^3B_1$ has so far been detected due to the fact that that the phosphorescence signal is relatively weak such that it is being swamped out by the stronger fluorescence background at high pressures and long lived triplet molecules suffer hetrogenous destruction at the walls of the cell as they diffuse out at low pressure condition. In the present work with the help of the supersonic jet, we were able to detect the $^3A_2$ system, whose presence was predicted by some workers. This was possible because in supersonic jet the molecules gain a large velocity component along the axis of the expanded jet and hence the the diffused $^3A_2$ molecules seemed to have been confined inside a limited volume

around the exciting beam such that their decay could be detected under optimum optical alignments.

CHAPTER III

EXPERIMENTAL

The experimental set up involves three major parts 1) Laser system 2) Molecular beam apparatus 3) Signal acquisition and processing unit. The schematic diagram for the entire experimental set up is shown in figure 3.1. The following sections describe in detail each part.

3.1 Laser System

The laser system employed in this work is the Quanta Ray system, which consists of a Q- switched Nd:YAG laser with a repetition rate of 10 Hz, A PDL-1 tunable dye laser and a wavelength extender (WEX). The 1064 nm infra - red (IR) fundamental generated by the Nd:YAG laser is frequency doubled by a HG-2 harmonic generator and the 532 nm beam thus obtained, is separated from the fundamental by a prism harmonic separator (PHS). The 532 nm beam was used to excite a tunable dye laser PDL -1 in the red region of the spectra. The output wavelength of the dye laser is controlled either manually or by a computer through a driving motor controlled interface (MCI). The output of the PDL-1 enters

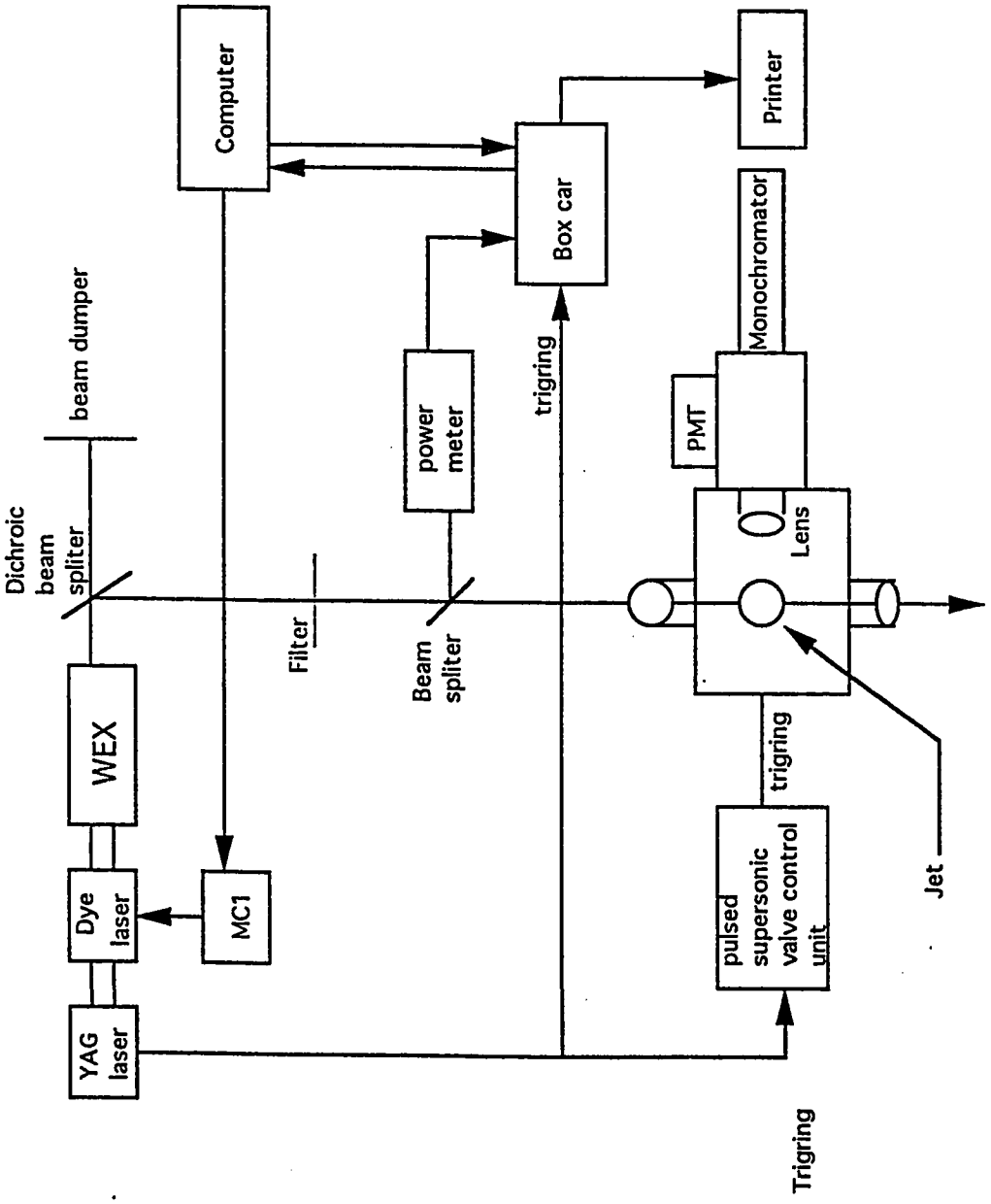

Figure 3.1 Schematic diagram of the Experimental set up

into the WEX, whose function is to frequency double the red wavelength radiation and to keep the intensity of the beam in the optimum condition as the PDL-1 dye laser is scanned. The output from the WEX, after passing through appropriate UV pass absorption filter, then vertically intercepts the molecular beam expanded from the supersonic jet. Each individual key unit in our laser system is described in detail as follows.

3.1.1 Nd:YAG laser.

Nd:YAG is the acronym for the Neodymium doped Yttrium Aluminum Garnet, the material of which the laser rod is made. Nd:YAG laser is the four level system as depicted by a simplified energy level diagram in figure 3.2. The Nd:YAG crystal is excited by a flash lamp, from which the crystal absorbs energy and is excited to $4F_{5/2}$ and $2H_{9/2}$ levels and subsequently crosses over to $4F_{3/2}$ state by radiation less transitions. The fluorescence occurs from $4F_{3/2}$ level to the four multiplets of the ground state, of which the probability of transition to $4I_{11/2}$ is more than any other members of the multiplet. $4I_{11/2}$ level is about 200 cm^{-1} above the ground state and hence at room temperature this level is virtually empty. So any population in the level $4F_{3/2}$ gives rise to a population inversion. The laser transition from $4F_{3/2} \rightarrow 4I_{11/2}$ corresponds to the laser radiation of wavelength 1064 nm whose line width is 6.5 cm^{-1}. The

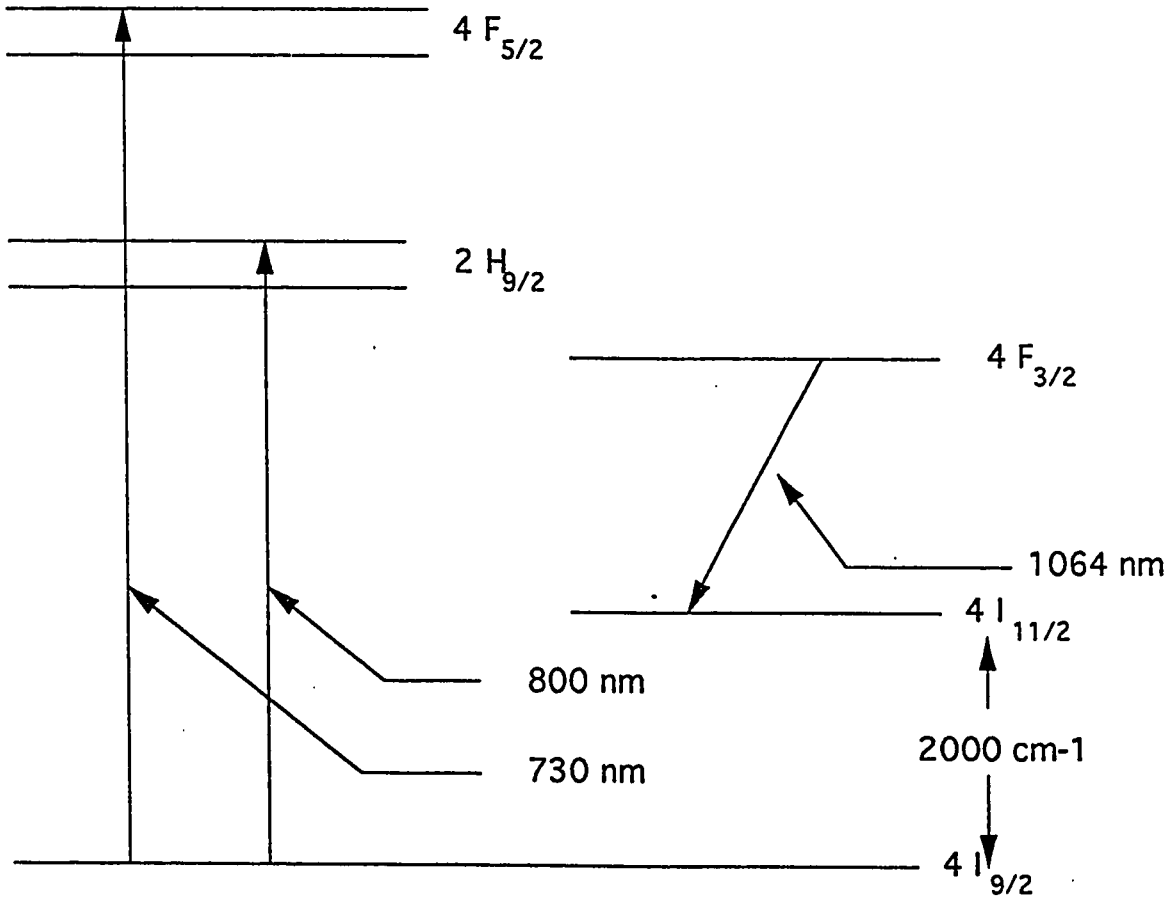

Figure : 3.2 Typical energy level diagram of Nd: YAG

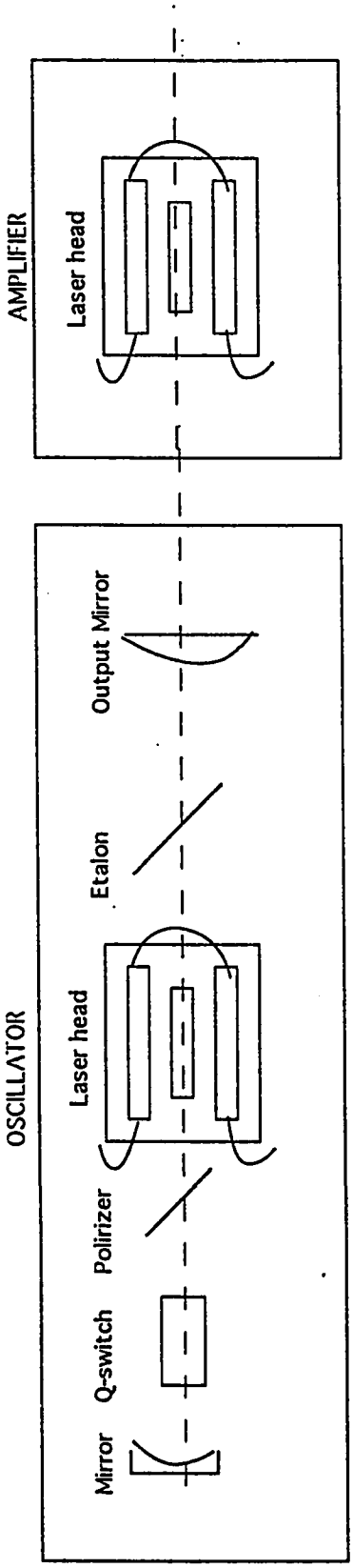

Figure : 3.3 Schematic diagram of the Nd:YAG laser system

lifetime of $4F_{3/2}$ level is 230 micro seconds. Transition from $4I_{11/2}$ to the lower levels take place by non radiative process and is quite fast.

The laser resonator in the Nd:YAG system is an unstable or Diffraction Coupled Resonator (DCR). The laser resonator with components such as a Q - switch, polarizer, and etalon complete the optical system. The flash lamp laser rod assembly is positioned in between the polarizer and the etalon as shown in figure 3.3. The flash lamp is driven by the discharge current of pulse repetition frequency 10 Hz and pulse duration 210 micro seconds. Q - switch works on an electro optical principle. When the crystal in the electro-optic cell is exposed to the electric field it becomes birefringent, i.e. the crystal medium is characterized by two orthogonal directions "fast" and "slow" axes, which has two different indices of refraction [30]. The laser beam, initially plane polarized by a polarizer at 45° to these axes, will hit the crystal normal to the crystal plane and will split into two orthogonal components, traveling along the same path but at different velocities. Hence a path difference is introduced between these beams. After travelling through the medium the two components will either circularly or elliptically or linearly polarized, depending on the voltage applied to the crystal. In Q - switch of Nd: YAG laser, during the flash lamp pulse a voltage $V_{1/4}$ is applied in such a way that the emerging beam out of the crystal will be circularly polarized with a wave retardation of $\lambda/4$. This beam is reflected by the end mirror and again passes through the electro optical cell. This time the beam will be

linearly polarized with another wave retardation of $\lambda/4$ and is ejected by the cavity. Towards the end of the flash lamp pulse the voltage in the cell is switched off, permitting the polarizer cell combination to pass a linearly polarized beam through the etalon without loss. The oscillation within the cavity will build up and after a delay, a Q - switch pulse will be emitted from the cavity with the high power. In order to get high power and good spatial profile of the beam, the end mirrors and the flash lamp Q- switch time delay need to be adjusted.

The 1064 nm beam thus produced in the Nd:YAG oscillator is power amplified with the Nd:YAG amplifier. The amplifier is just a the laser rod positioned in between two flash lamp. The pulse repetition frequency and the pulse width of the flash lamp pulse is same as that of the oscillator. In the Nd:YAG Oscillator - Amplifier system, pulse width, beam divergence and beam spatial width are primarily determined by the oscillator where as the pulse power and pulse energy are determined by the amplifier.

3.1.2 Harmonic Generator and Prism Harmonic Separator.

In the Nd:YAG laser system we can get only laser radiation of single wavelength (1064 nm). By using the principle of harmonic generation by nonlinear optical crystals such as KD*P, second, third harmonics of 1064 nm can be produced. When the laser radiation of

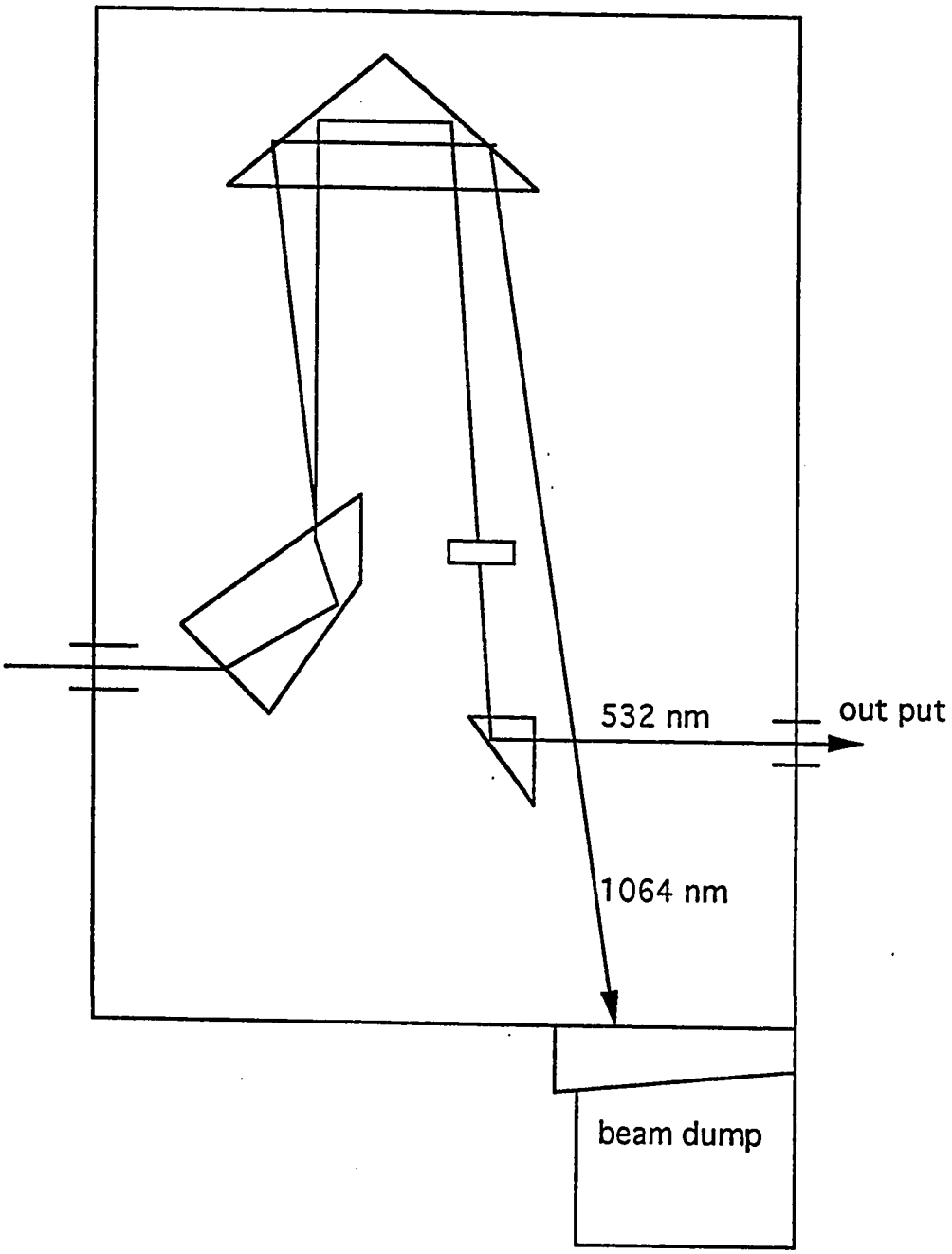

Figure : 3.4 Prism Harmonic Separater

frequency ω hits the KD*P crystal, dipole polarization will take place due to the presence of the electric component of the laser radiation [31]. This polarization oscillates with a frequency 2ω and radiates the electromagnetic wave of frequency 2ω, which propagates with the same characteristics as that of the incident laser light. The wave thus produced has the same characteristics of directionality and monochromaticity as the incident wave and is emitted in the same direction. This phenomenon is known as the second harmonic generation.

In the harmonic generator the KD*P crystal is placed inside a metallic housing. The 1064 nm beam from the Nd:YAG enters the polarization rotator, which is adjusted to rotate the polarization of the 1064 nm beam so as to achieve optimum harmonic generation with maximum power. There is also an angle tune knob which adjusts the angular orientation of the crystal for optimum phase matching and thereby to give maximum power output.

The output from the harmonic generator (HG-2) contains both 532 nm and 1064 nm beams which are separated by means of the Prism Harmonic Separator (PHS). The various optics involved in the PHS are shown in figure 3.4. The output from the HG-2 is directed on the input face of the Pellin - Broca prism. After passing through the Pellin - Broca prism the 532 nm and 1064 nm are separated and are directed onto the roof prism . Then the 532 nm laser radiation is passed through the half-wave plate and used to excite the dye laser, whereas the 1064 nm beam is

Table - 3.1

Secifications of Nd:YAG for the present experiment.

Flash lamp pulse repetition frequency	:	10 Hz
Flash lamp pulse width	:	210 μs
Q - switch pulse repetition frequency	:	10 Hz
Q - switch pulse width	:	20 ns
Pulse width of 532 nm beam	:	6 - 7 ns
Line width of 532 nm beam	:	6.5 cm^{-1}
Power of the 532 nm beam after passing through the PHS	:	400 mj

dumped in the beam dump. The specifications of the Nd:YAG laser for the present experiment are listed in table 3.1.

3.1.3 Tunable Dye Laser

Nd:YAG laser is capable of producing the laser beam of wavelength 1064 nm or the second and third harmonics of 1064 nm. To work at any other wavelength from ultra-violet to mid-infra red the tunable dye laser excited by the Nd:YAG laser must be used with appropriate dye. The combination of Nd :YAG and PDL - 2 pulsed dye laser provides the tunable laser radiation from 380 nm to 960 nm. The tuning range is even further extended from 190 nm in UV to 4500 nm in mid-infra red through nonlinear optical process in wavelength extender.

To explain how the laser action takes place in a dye laser a typical energy level diagram of an organic dye molecule is shown in figure 3.5 [32]. It consists of electronic ground state (S_0) and a number of excited singlet states (S_1, S_2, ...) with a number of triplet states (T_1, T_2 ....). Typically the spacing between two adjacent vibrational levels is about (1400-1700 cm^{-1}) and between two adjacent rotational level is about 14 -17 cm^{-1}, and between electronic energy level separation is 20,000 cm^{-1}

The basic process of laser action begins with pumping the dye with an excitation source that excites their molecules from lowest level (A) of the ground state (S_0) to the higher vibrational rotational levels (b) of

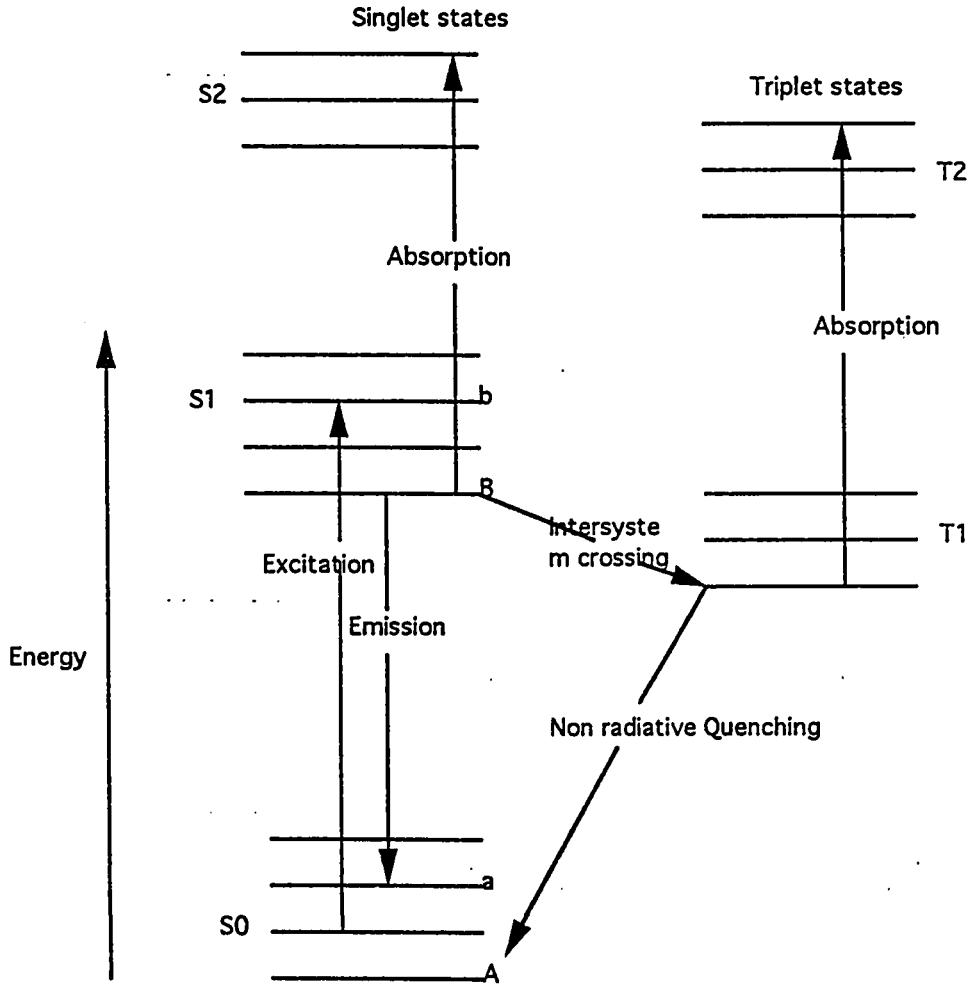

Figure: 3.5 Typical energy level diagram of an organic dye

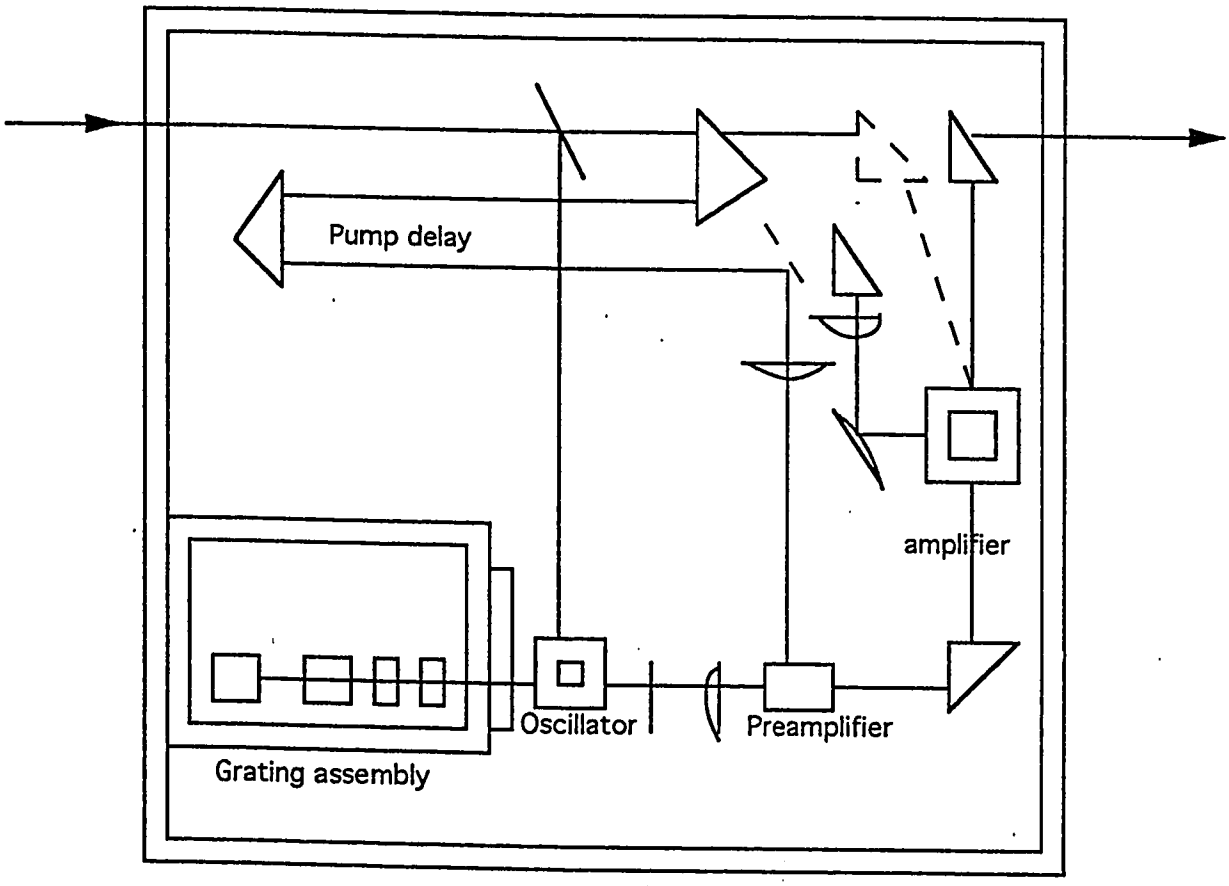

Figure : 3.6 Dye laser schematic diagram

the singlet states (S_1). This transition is indicated as (A-b). The rapid collisions with other molecules take place and releases of the excess energy of the excited molecules to the lowest vibrational level (B) of the state (S_1) in a time of the order of (10^{-11}-10^{-12} sec). This process is marked by (b-B) process. The laser action takes place when the molecule decays either by spontaneous or stimulated emission to one of the rotational vibrational level of the ground state with the radiative time of about 10^{-9} sec. This process is designated by (B-a). Finally a non radiative decay takes the molecule back to the lowest level (a) of the ground state due to the rapid non radiative process (b-B) and (a-A). The efficiency of the laser action can be reduced or quenched by several processes that competes with the fluorescence decay modes of the molecules. The most important process is the non radiative process to go to the ground state (S_1-S_0) and non radiative intersystem crossing (S_1-T_1).

The shematic diagram of the PDL- 2 is given in figure 3.6. In standard configration PDL -2 consists of an oscillator, an end pumped final amplifier, and pump beam distribution optics. A small fraction of the pump beam is split off to excite the oscillator the reminder excites the amplifier. The optical layout of the oscillator is shown in figure 3.7. The oscillator is a monochromator coupled to a gain medium and consists of a output coupler, a dye cell, and a prism beam expander. This design has the advantage of having high efficiency and broad tuning range with a single grating.

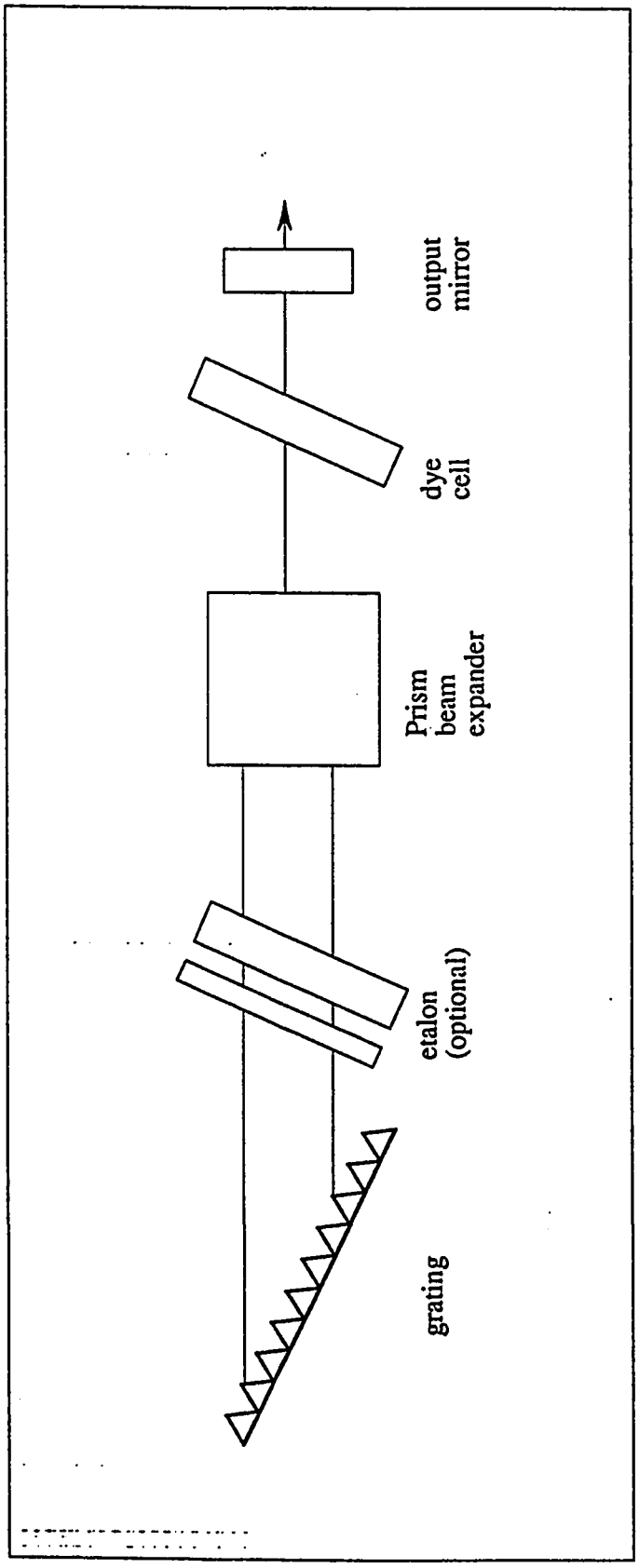

Figure : 3.7 Oscillator of the dye laser

Table 3.2

PDL - 2 Dye laser specifications for this work.

Dye used	:	Sulforhodamine 640	
Concentration	:	90.9 mg / lit	(oscillator)
		13.6 mg / lit	(amplifier)
Solvent	:	Methanol	
Pre amplifier	:	No	
Etalon	:	No	
Pump wavelength	:	532 nm	
Pump energy	:	400 mj	
Peak wavelength	:	608 nm	
Efficiency	:	13.25%	
Power out	:	53 mj	
Pulse width	:	6 ns	

In the oscillator the grating disperses the light. Depending on the orientation of the grating, emission over only a narrow wavelength band will be reflected back into the oscillator cavity, providing the required feed back to achieve lasing. The absolute wavelength is therefore the function of the grating angle. By using different orders of the grating the dye laser can be tuned from 380 nm to 960 nm. Rotating the grating for tuning can be done by a stepper-motor, which is controlled by the motor controlled interface (MCI). The prism beam expander elongates the beam to illuminate all grating grooves. Proper filling is critical to obtain narrowest linewidth. The linewidth can be further reduced by the use of optional air spaced etalon.

The dye solution is prepared and stored in two teflon containers of the dye circulator. The name of the dye and the concentration of the dye solution for oscillator and amplifier are listed in the system specification of the dye laser in table 3.2. In order to achieve maximum power output of the dye laser, the beam has to hit each individual optics exactly at the optical center, and hence both horizontal and vertical translation of each optics is finely adjusted to achieve maximum power.

3.1.4 Automatic Tracking Wavelength Extender (WEX)

The tuning range of the dye laser system can be extended with a wavelength extender. This wavelength extension is achieved either by

doubling the dye laser output through non-linear optical process or by mixing the dye laser output with the 1064 nm fundamental coming directly from the Nd:YAG laser. For the present experiment we doubled just the dye laser wavelength. Another important function of the WEX is to keep the laser output in the optimum position as the dye laser is scanned.

The mechanism of frequency doubling in the KD*P crystal is the same as the one discussed in the second harmonic generation. As the dye laser is scanned the power output of the crystal will fluctuate due to lack of phase matching. So orientation of the crystal has to be automatically adjusted so as to achieve a good phase matching and hence optimum power. This is achieved by a photo diode and servo motor combination which is technically known as tracking. The laser beam after passing through the doubling crystal falls onto the photodiode. If the spatial distribution of the beam is not uniform due to lack of phase matching, the photo-detector will send a signal to drive the servo motor which in turn change the orientation of the crystal to achieve maximum phase matching. The output of the PDL-2 is directed on one of the beam combiners (BC-0, BC-1, BC-2, and BC-3) which is selected according to its active wavelength region. The beam from the beam combiner falls on the doubling crystal housing where a set of crystals (C_1 through C_7) is located, from which the appropriate crystal is chosen to cover the desired wavelength. For the present work the beam combiner BC-2 and the crystal C-2 were used because the tuning range of the sulforhodamine 640 falls on the effective wavelength range of BC-2

and C-2. After passing through the crystal the beam is taken out either by using output prism or by Pellin - Broca prism. The power of the output beam can be increased by adjusting the output prism. The laser beam output of the WEX is passed through the UV pass filter to cut off all the non - UV radiation and the beam is focused to the molecular chamber with a focusing lens.

3.2 Molecular Beam Apparatus or Supersonic Jet System

3.2.1 Cooling Mechanism in supersonic jet

In a supersonic jet, the molecules flow from the high pressure reservoir to the low pressure region through an orifice whose diameter is greater than the mean free path of the molecules in the reservoir. This allows for many collisions in and down the stream of the orifice, imparting large velocity component along the axial direction. Thus the random molecular motion is converted into a directed mass flow.

The directed mass flow has three consequences: first the peak of the molecule's velocity distribution along the axis is shifted to the higher velocity and the width of this velocity distribution is narrowed down. That is the velocity of the molecule is increased accompanied by a drastic reduction in the temperature characterizing the distribution. Thus the Mach number (M), defined as the ratio of molecular velocity to the local

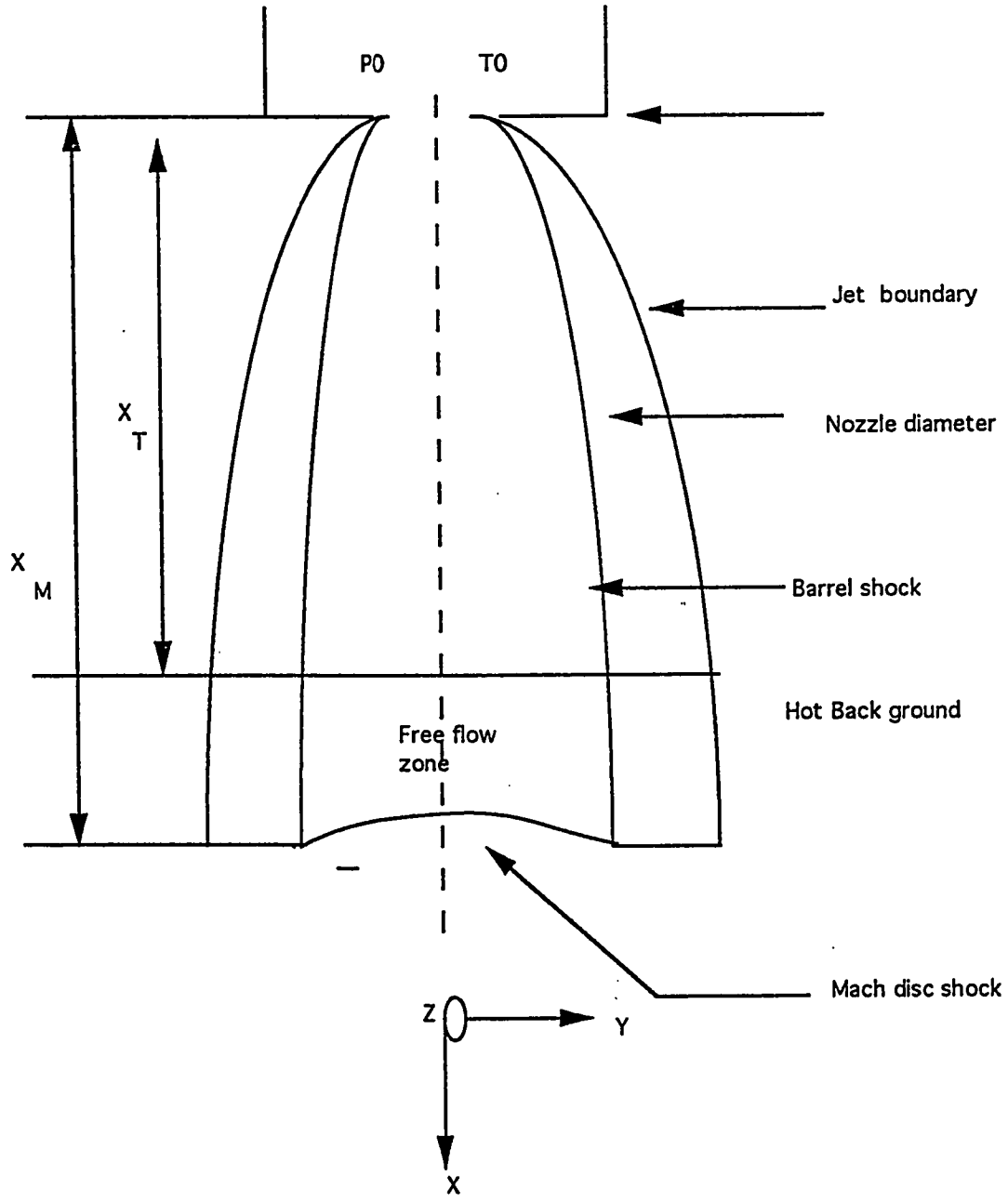

Figure : 3.8 Supersonic beam profile

speed of sound is increased; M > 1. The second consequence is that the beam intensity is enormously increased which is the primary motivation for the development of supersonic nozzle beam source.

The third and very important consequence as far as spectroscopic applications are concerned is that the initial part of the expansion is isentropic in nature, i.e. there is an equilibration between the tanslational and internal degrees of freedom. At the isentropic core of the jet the temperature characterizing the vibrational and rotational energy distribution will decrease. As the collision frequency decreases the vibrational as well as rotational temperatures begins to lag behind the translational temperature, and eventually as the collision frequency becomes negligible, the molecules enter into a free flow zone through which no furthur cooling takes place. In figure 3.8, the point X_T marks the beginning of the free flow zone of the typical expansion condition, which constitutes the ideal spectroscopic region .

In the supersonic jet system, the fluorescence detecting system is perpendicular to the direction of molecular flow and therefore, since the molecules encounter small velocity component along the direction of the detector, Dopppler broadening becomes negligible. This is desirable especially when analyzing the rotational structure of light molecules.

The SO_2 sample used in the present experiment was of high purity (99.97%), provided by Air product, UK. Further vibrational and rotational cooling was achieved by seeding SO_2 into monoatomic gas such

as Ar. The purpose of seeding is to increase the flow and thereby increasing the Mach number (M). Moreover the orifice of the jet is a pulsed one. The advantage of using the pulsed valve is to reduce the pumping requirements drastically and also to conserve the sample.

3.2.2 Molecular Beam Apparatus.

The molecular beam is produced through a Newport BV100 pulsed molecular beam valve, which is capable of producing the short duration high speed gas pulse. The BV100 consists of BV100V valve, and BV100D driver. The BV100 generates pulses, producing molecular beams cooled rotationally to as low as 3K thereby reducing the hot band absorption and allowing the increased spectral resolution.

The BV100 consists of a dual electromagnet actuator assembly housed in a 1.25 inch diameter stainless steel cylinder. The housing is flanged at one end to carry gas inlet ports and electrical feedthrough connections. Mounted at the other end is the removable end plate which contains the valve orifice. The valve is mounted on a vacuum chamber with orifice end protruding through a common feedthrough fittings.

The beam valve is divided into two chambers separated by a bellow diaphragm as shown in the figure 3.9. The sample gas chamber carries the gas to be metered by the valve. All the materials exposed to the sample gas are corrosion resistant. The backing chamber carries N_2, at

pressures necessary to balance the differential pressure across the bellow diaphragm. The actuator assembly drives a polymer seal tip against the orifice to close the valve. Actuator stroke can be controlled from the BV100D driver.

The BV100 driver is an AC line-powered controller, which provides proper current level and pulse timing sequence to the two actuator coils in the beam valve. This BV100D is triggered by the oscillator of the Nd:YAG laser with the frequency 10 Hz. The driver contains an internal pulse rate generator, a trigger delay generator and timer for the coil current pulse width and timing control. The pulse repetition rate and duration can be adjusted and can be monitored on a cathode ray oscilloscope.

A stainless steel chamber with high vacuum connections can be used to prepare and store the sample gas/carrier gas mixture to be introduced into the valve. Another alternative method used in this work is the on-line sample mixing, in which the high purity (99.97%) SO_2 at the pressure of 35 psi is mixed with the carrier gas Ar at the pressure of 30 psi. The adjustable needle valve, which is properly calibrated, is used to monitor the mixing ratio. There are two factors that control the concentration of SO_2. Since the carrier gas stagnation pressure and the diameter of the nozzle are fixed, the Mach number (M) at a distance X from the nozzle along the axis of the jet depends only on the value X [33]

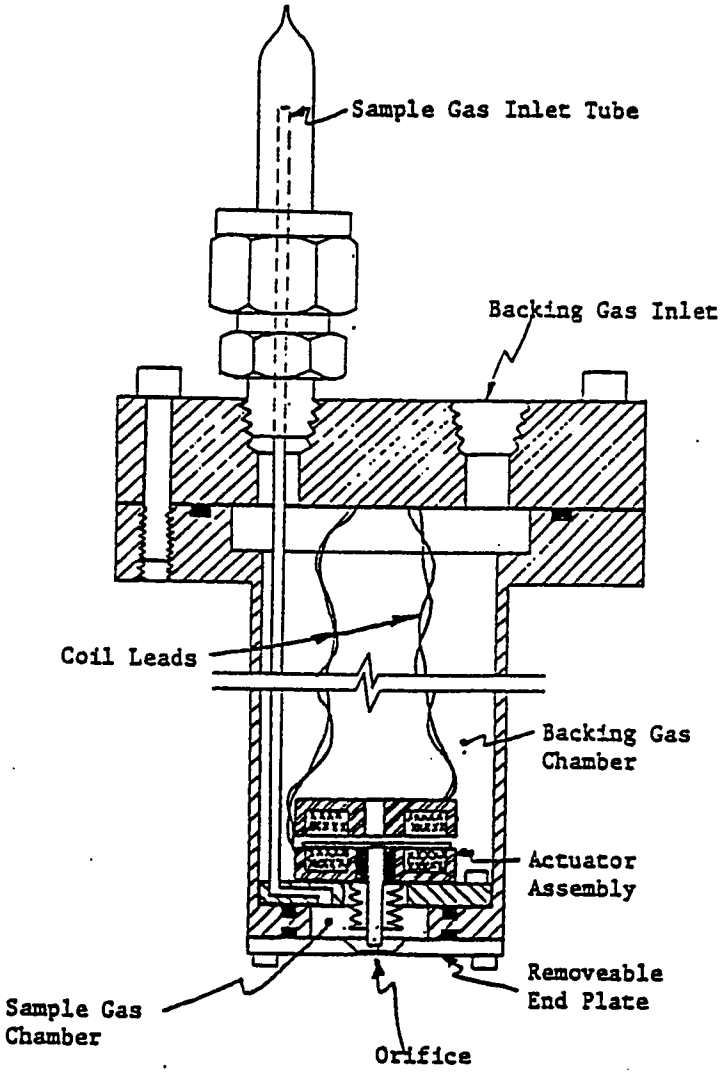

Figure : 3.9 BV- 100V Valve of supersonic jet.

$$M = 3.26 \left(\frac{X}{D}\right)^{0.67} \qquad (3.2.1)$$

The schematic diagram for typical supersonic expansion is shown in figure 3.8. The density of Ar and SO_2 mixture as well as the collision rate and temperature decreases with increasing distance X until a limit beyond which these parameters reach their terminal value (inside the free flow zone) The terminal value of the Mach number is given by [33]

$$M_T = 133\ (P_0\ D)^{0.4} \qquad (3.2.2)$$

where P_0 and D are in atm and cm respectively. The terminal distance X_T may then be calculated by substituting the value of M_T into the equation 3.2.1. In the present experiment the terminal values of th Mach number M_T and the X distance X_T were always fixed at 52 and 1.9 cm respectively. The luminescence spectra were recorded at a set of X values equal to 2, 5, 10, 20 mm which produced Mach number equal to 12, 21, 34, and 52 respectively. These values were used to estimate the molecular density at the corresponding X values by using the relation [33].

$$n = \frac{n_0}{\left[\,1 + 0.5\,(\gamma - 1)\,M^2\right]^{1/(\gamma - 1)}} \qquad (3.2.3)$$

where $\gamma = 1.67$ and $n_0 = 7.5 \times 1019\ cm^{-3}$ is the mixture density at P_0 and T_0, the room temperature.

Therefore the corresponding densities at the above X values could be estimated as approximately $2.5x10^{17}$, $4x10^{16}$ $1x10^{16}$ and $2.5x10^{15}$ cm^{-3} respectively. By varying the SO_2 concentration while keeping the X distance fixed one can vary the SO_2 partial pressure at the point of excitation while keeping the SO_2 + Ar pressure constant. For example, the ratio $[SO_2]/[Ar] = 0.02$ and distance X = 10 mm give an SO_2 partial pressure of 6.5 mtorr within 0.3 torr of total Ar + SO_2 pressure. If X is kept fixed at 10 mm and the $[SO_2]/[Ar]$ ratio is for example decreased to 0.01 then the total pressure would remain 0.3 torr but the SO_2 partial pressure would decrease to 3 mtorr. Varying the X distance while keeping the $[SO_2]/[Ar]$ constant, on the other hand would vary both the SO_2 pressure as well as the total pressure of the mixer. For example, at X = 5 mm and $[SO_2]/[Ar] = 0.02$, the SO_2 pressure would be 25 mtorr and the total pressure would be 1.2 torr. It should be stated that the above equations are valid only for the monoatomic gases. For the polyatomic gases, these expressions offer reasonable approximation only when the poly atomic gases are seeded in the mono atomic carrier gases as in the present experiment.

The X distance is varied by sliding the pulse valve on a vacuum sealed XYZ mount rather than by tilting the laser beam. Thus, to ensure an untilted beam path such that he excitation point is always fixed at

a given X distance, the laser beam is allowed to pass through a set of four light baffles along the Y axis inside the vacuum chamber and to be monitored at a screen outside the opposite window. In this case the point of excitation is exactly in front of the spectrometer's field of view, allowing the fluorescence from the short lived excited molecule to be excited. When monitoring the Phosphorescence from the triplet molecules at low concentration, on the other hand, the exciting beam was deviated such that it passed just outside the detection field of view. Thus the fluorescence of the short lived molecule was efficiently blocked while the phosphorescence of the long lived molecule as these molecules traveled in front of the field of view. This usually occurred when the laser beam after passing through the molecular beam was blocked by the body of the third or fourth baffle and did not go through the opposite window. In this case care was taken to minimize the undesirable scattered laser light such that the signal to noise ratio was always better than 95%. Also, to ensure the stable [SO_2]/ [Ar] ratio after each needle valve setting, sufficient time was always given before the actual recording of the spectra for each concentration.

The jet expands from the valve into an evacuated chamber equipped with two pairs of mutually orthogonal opposing portals. One pair is used for fluorescence detection, where as the other pair has Brewester angle quartz window to allow maximum transmission of UV excitation beam. In order to minimize the laser light scattering into the

fluorescence detection optics, one pair of light baffle is inserted in the pair of portals through which the laser enters.

The molecular beam / fluorescence chamber is evacuated by a microprocessor controlled vacuum system that includes a 6 inch diffusion pump and a rotary backing pump, both from Edwards. The vacuum system is capable of maintaining the pressure of 10^{-3} mbar during the operation of the valve. A Varian vacuum pump system is used to enhance the mixing of SO_2 and Ar by air release and to clean up the sample line before and after the experiment.

3.3 Data Aquisition and processing unit.

This system consists of a computer controlled spectrometer (SPEX 1870 0.5m), a photomultiplier (Thorm EMI), a boxcar integrator (EG&G Model 4422 with a model 4402) and a computer.

3.3.1 Spectrometer.

The schematic diagram of the 1870 series 0.5m spectrometer is shown in figure 3.10. It has an entrance and an exit whose width can be varied by adjusting the width of the entrance and exit slit with a micrometer screw adjustment. For the present work, the slit width was kept at 350 μm. A photomultiplier tube is attached at the exit of the

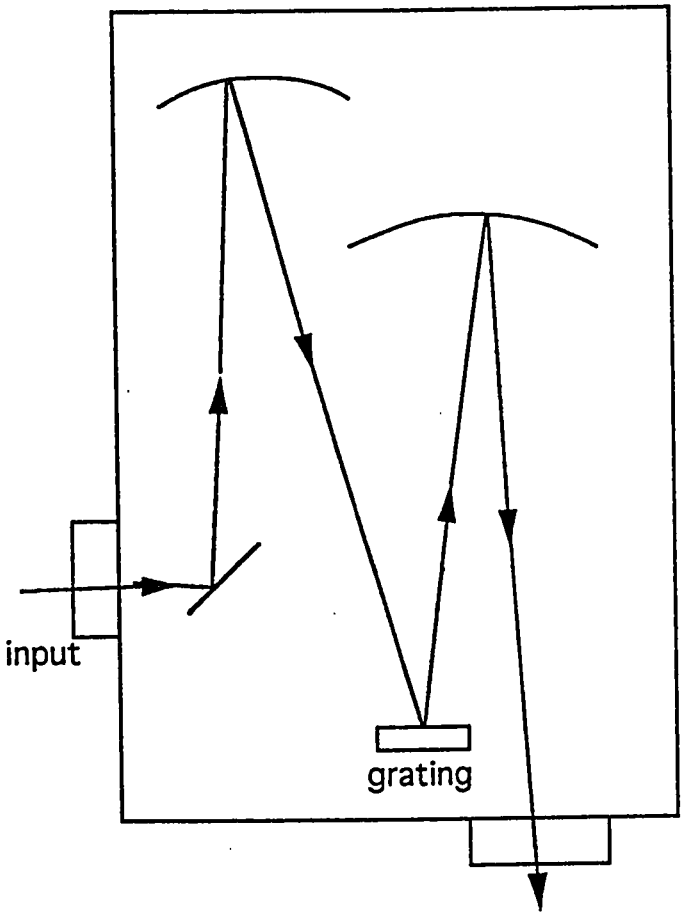

Figure : 3.10 Spectrometer schematic diagram

spectrometer. The fluorescence from the molecule is directed on the blazed grating of the spectrometer and then to the exit slit through the optical arrangement as shown in the figure 3.10. A monochromatic signal of desired wavelength (if available in the total fluorescence) can be allowed to pass through the exit slit by adjusting the grating angle in accordance with the blazed grating equation. This job is done by the CD- 2A compudrive, which is connected to the spectrometer. By using this compudrive, the monochromator can be set at a desired operating wavelength or it can be scanned between two wavelength limits with certain scan rate. The scan rate for the present experiment was 1Å / second. The operating wavelength at any instance can be read out from the analog display in the spectrometer and the digital display in the compudrive. The scan can be paused and repeated as desired by using the compudrive.

3.3.2 Photomultiplier Tube.

The photomultiplier tube (PMT) is based on the principle of photo-electric effect. The device consists of a cathode, a series of dynodes and focusing elements. A high voltage is supplied to the cathode with a high voltage variable power supply. When the molecular fluorescence falls on the cathode the photoelectrons are ejected and are focused on the first dynode by the presence of the electrostatic field. Subsequently the photo electrons are accelerated between the successive dynodes, thereby

providing a current amplification. The PMT has two connections: one for high voltage supply and the another one to get the signal output.

3.3.3 Boxcar system

The boxcar system consists of two separate but interdependent instruments: the model 4420 boxcar averager and the model 4402 signal processor. Up to four gated integrated modules can be installed in the model 4420 main frame, allowing the detection of as many as four signals simultaneously. For the present work two modules were used. The boxcar averager is triggered by the Q - switch of the Nd:YAG laser system. The 4402 signal processor system contains a 68000 microprocessor, a 7 inch CRT display, a front panel key board, 5.25 inch floppy disk drive and multiple curve storage memories and registers. The 4420/4402 combination is interfaced with the external computer with the GPIB interface, enabling the system to be controlled externally by the computer. The data acquired through this system can be smoothed, analyzed. and stored in the floppy disk.

3.4 Different Experiments using these systems

Three modes of experiments were done using the above systems. 1) Excitation spectrum 2) Dispersed fluorescence spectrum 3) Excitation spectrum with monochromator.

3.4.1 Excitation spectrum

In this mode of experiment we are interested in collecting the total fluorescence of the molecule while the dye laser is scanned between two wavelength limits. The stepper motor of the dye laser is connected to the computer through the Motor Controlled Interface (MCI), and hence the scanning of the dye laser can be controlled by the computer with certain scan rate. The scan rate for the present experiment was 0.8 Å / second. The UV laser from the WEX hits the molecule vertically. The total fluorescence from the molecule is focussed to the PMT directly, and the signal from the PMT is fed to the Boxcar system. If there is any absorption at a particular wavelength, due to total fluorescence there will be a peak appearing at that wavelength. The other channel of the boxcar is connected to the ScienTech 361 power meter, which monitors the laser power after passing through the molecular chamber. This is used for the power normalization purposes. The collected data from the boxcar can be dumped to the computer for analysis [34]. Dumping and analysing of the data in the

computer enables us for efficient data analysis and to minimize the wear and tear of the boxcar system.

3.4.2 Dispersed fluorescence Spectrum.

In this mode of experiment, the molecule is excited by the laser beam of single wavelength corresponds to any peak of the excitation spectrum, while the monochromator is scanned between two wavelength limits. When the molecule is excited to certain level, it decays to all possible lower levels emitting the corresponding wavelength. In this mode of experiment the fluorescence from the molecule is fed into the spectrometer, which is connected to the PMT and then to the boxcar integrator. If there is any fluorescence or phosphorescence of particular wavelength is present as the monochromator is scanned, a peak will appear in the dispersed fluorescence spectrum. In this experiment also the data from the boxcar system is dumped into the computer for data analysis. The scanning rate of the monochromator is 1Å / second.

3.4.3 Excitation Spectrum with Monochromator.

In this mode of experiment we monitor which excitation wavelengths are responsible for the emission of a particular wavelength. Hence the monochromator is fixed at a particular wavelength whereas the

dye laser is scaned between certain wavelength limits. In this experiment also the fluorescence is directed to the entrance slit of the spectrometer and the signal is acquired through the PMT and the boxcar system.

CHAPTER IV

RESULTS AND DISCUSSIONS

As mentioned in section 2.9, the relatively long life-time of the $^1B_1(L)$ electronic state is due to its coupling with the triplet manifold. Caton and Gangadharan [10] reported that this coupling is relatively strong at 3021 and 3131 Å wavelengths in particular. They also observed an increase in the phosphorescence quantum yield at low pressures when 3021 Å and 3131 Å were used as the excitation wavelength. However no possible explanation for this phenomenon was suggested by them or by any other subsequent worker. In the present work, we study this phenomenon by exciting the fluorescence and phosphorescence of SO_2 with the 3021 Å laser radiation under low pressures.

4.1 Excitation Spectrum of the F - band Region.

Figure 4.1 shows the excitation spectra in the F-band region of jet cooled SO_2 recorded while monitoring the total fluorescence signal. The supersonic conditions were the same for both the spectra except that the concentration of SO_2 relative to the carrier gas was estimated to be about

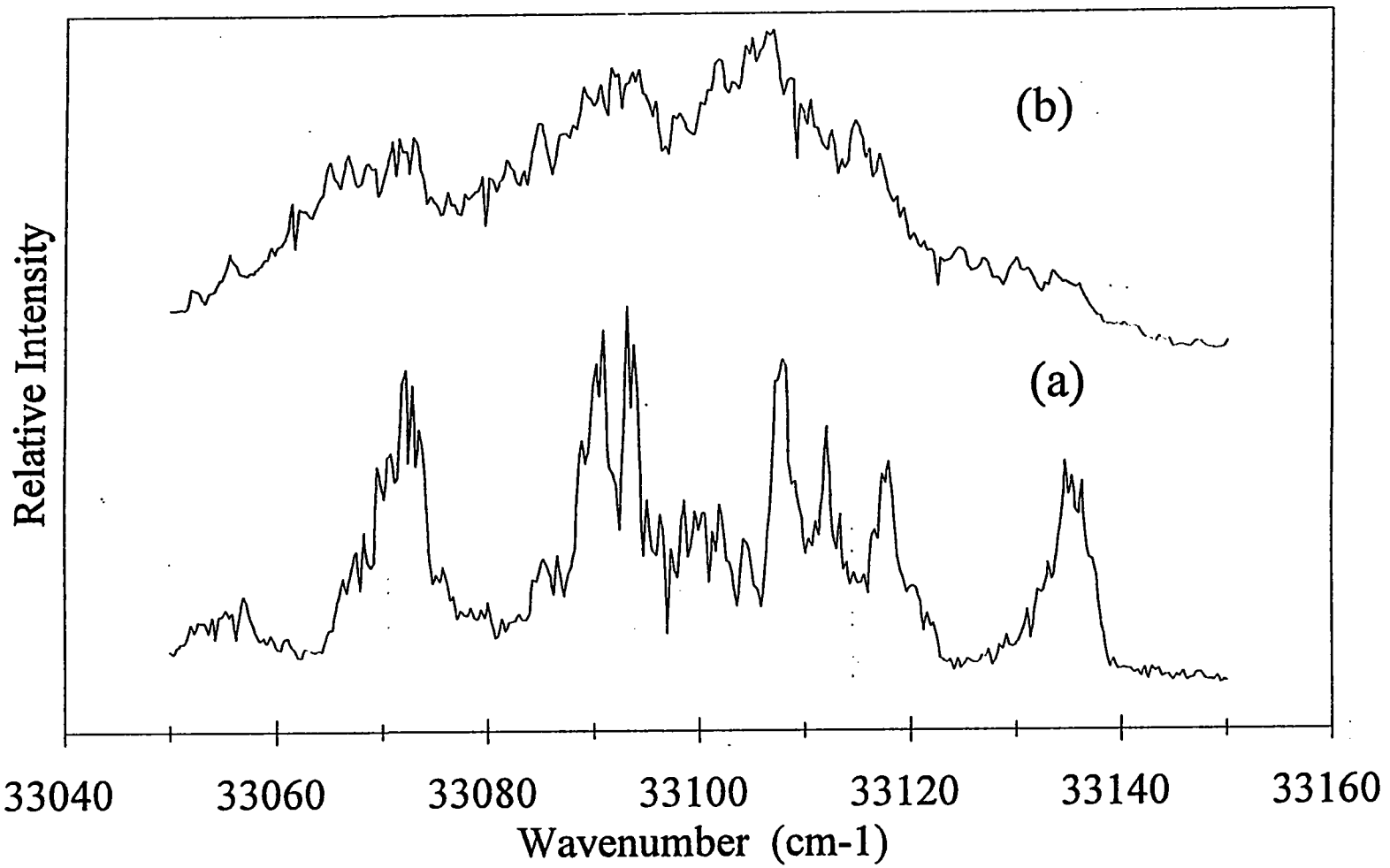

Figure : 4.1 Excitation spectra of the F-band region with SO_2 concentration >1% in (a) and 10% in (b). For both spectra laser to nozzle distance is 10 mm.

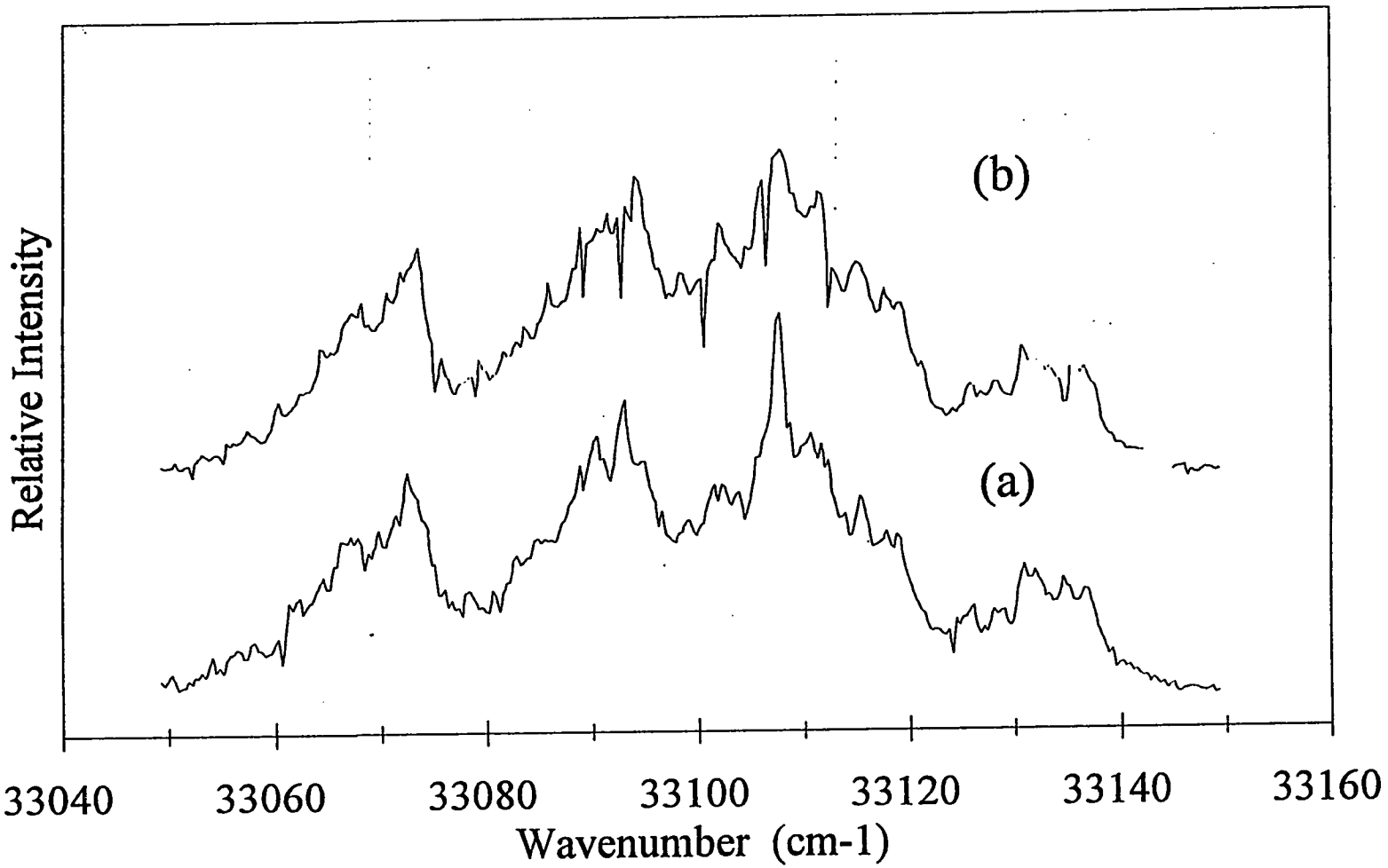

Figure : 4.2 Excitation spectra of the F-band region with nozzle to laser distance 20mm in (a) and 4 mm in (b). For both the spectra SO_2 concentration is 5%,

1% in (a) and 10% in (b). The dependence of rotational cooling on concentration discussed in section 2.8 is apparent here. The vibrational band widths show noticeable narrowing as the concentration is lowered. The effect of changing the nozzle to laser distance while fixing the concentration of SO_2 can be seen in figure 4.2. Here the concentration of SO_2 was fixed at 5% but the nozzle to laser distance was kept at 20 mm in (a) and 4 mm in (b). By comparing these two spectra, one can notice that, although there is some degree of rotational cooling at larger laser to nozzle distance, this cooling is not as efficient as in the case of changing the concentration. This leads us to think that the rotational cooling may be enhanced through SO_2 - Ar collisions rather than through SO_2 - SO_2 collisions.

The Mach number (M) for a supersonic beam, expressed in equation 3.2.1, is a function of the nozzle to laser distance only, for a particular nozzle diameter. Therefore, the total SO_2 + Ar, molecular density can be varied by varying the nozzle to laser distance alone, for a fixed mixture density and nozzle diameter. Thus it is evident that by varying the SO_2 concentration while keeping the nozzle to laser distance fixed, one can vary the SO_2 partial pressure at the point of excitation, while keeping the total SO_2 + Ar pressure almost constant. On the other hand by varying the nozzle to laser distance while keeping the SO_2 concentration constant would vary both the SO_2 partial pressure and the total pressure of the mixture. In figure 4.1, as we decrease the SO_2 concentration for a fixed

(X), SO_2 partial pressure is decreased and hence SO_2 - Ar collisions are expected to increase with respect to SO_2 - SO_2 collisions. Whereas in figure 4.2, as we increase the nozzle to laser distance for a fixed SO_2 concentration, both SO_2 partial pressure and the total SO_2 + Ar pressure is decreased and hence there is no appreciable increase in the SO_2 - Ar collision with respect to SO_2 - SO_2 collision. Therefore we can expect that SO_2 - Ar collisions are much more effective in the rotational cooling than SO_2 - SO_2 collision .

4.2 Detection of $^3A_2$ at low pressure.

Figure 4.3 and 4.4 show the emission spectra of SO_2 when excited by 3021 Å laser radiation in an expanded jet beam under two different conditions of optical alignment of the detecting system. For both figures the SO_2 concentration was o.3% and the nozzle to laser distance (X) was 5 mm which corresponded to the SO_2 pressure of about 3.5 mtorr and the total SO_2 + Ar pressure of 1.2 torr. Figure 4.3 represents the resonance fluorescence spectrum of the excited F-band (due to equation 2.10.4) which was detected when the point of excitation was exactly in front of the spectrometer's field of view. Figure 4.4 on the other hand depicts a completely different system of vibrational transitions recorded when the exciting laser beam was allowed to pass just outside the

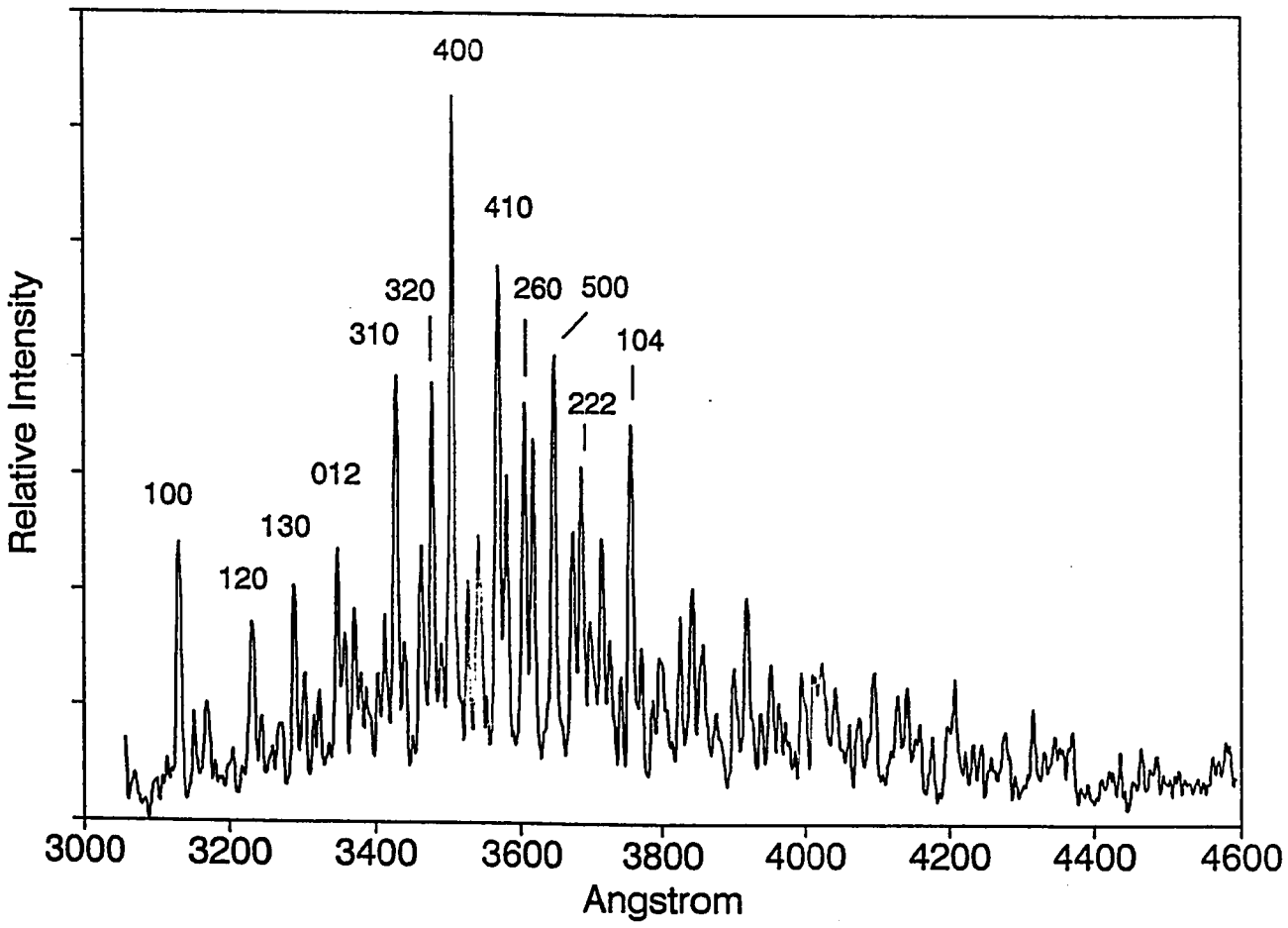

Figure : 4.3 (a) Resonance fluorescence spectrum of the excited F - band at 3021 Å. The SO_2 concentration was 0. 3% and nozzle to laser distance X was 5mm. The numbers represent the lower vibrational levels of $^1A_1$ state into which some prominant transition terminate.

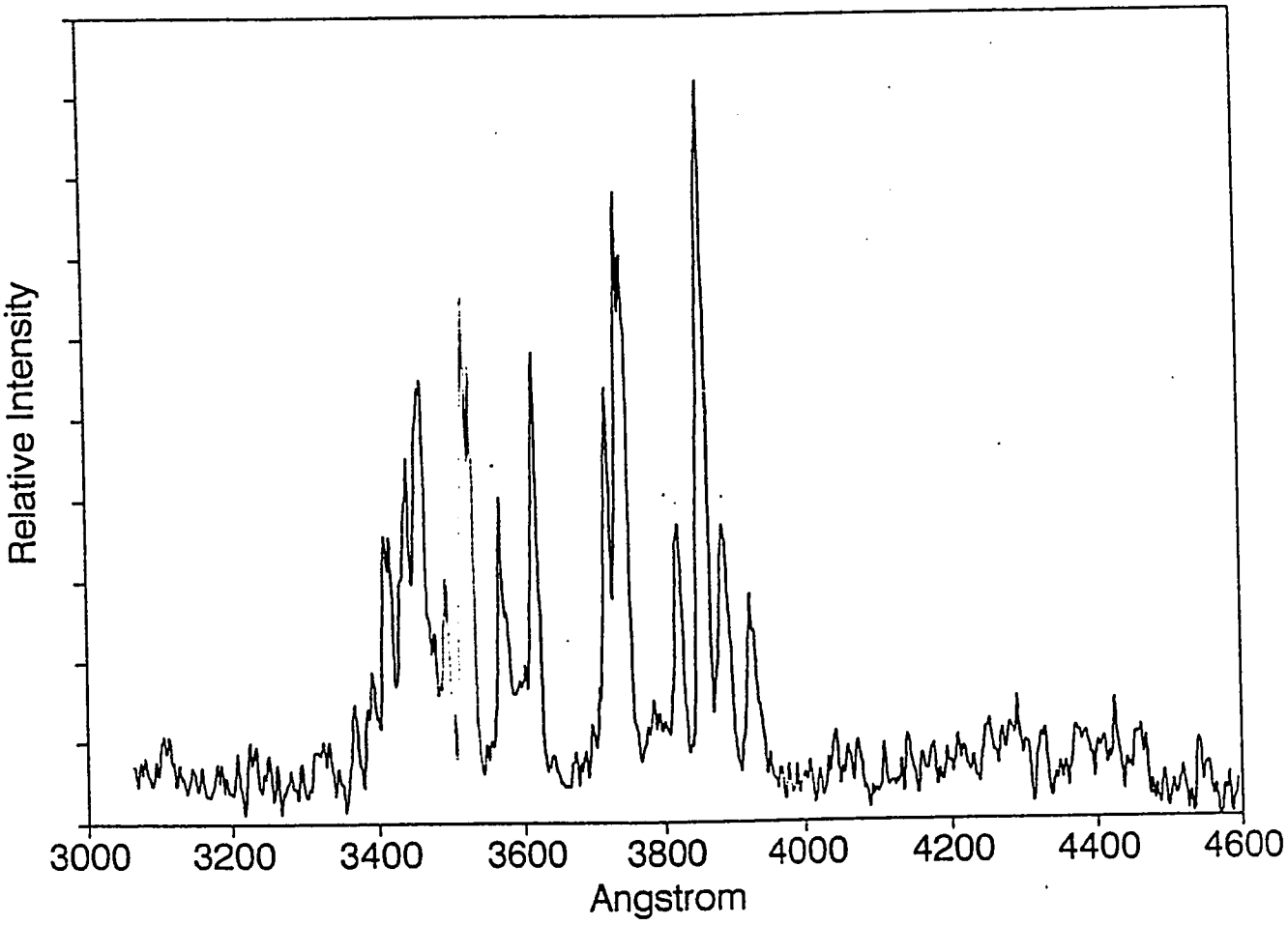

Figure : 4.4 Phosphorescence spectrum from long lived triplet molecules. The excitation wavelength and the concentration conditions are same as in figure 4.3.

spectrometer's field of view and are apparently due to the phosphorescence of the long lived-triplet molecules.

Figure 4.3 also shows the identification of the prominent vibrational transitions from the F band's upper level to various ground state levels. This vibrational analysis was carried out with 5 cm^{-1} accuracy using the anharmonic expansion of vibrational energy.

$$G(v_1, v_2, v_3) = \sum_i \omega i\,(v_i + o.5) + \sum_{i \le j} X_{ij}\,(v_i + 0.5)\,(v_j + 0.5) + \sum_{i \le j \le k} Y_{ijk}\,(v_i + 0.5)\,(v_j + 0.5)\,(v_k + 0.5) \qquad (4.1.1)$$

where the various vibrational parameters of the ground state were taken from the stimulated emission pumping work by Yamanouchi et al [20]. The vibrational analysis scheme for the resonance fluorescence of F-band is listed in table 4.1, in which few v_1, v_2 and v_3 progressions of the ground state are present. As the concentration of SO2 was gradually increased the intensity of the background fluorescence emission (given by equation 2.10.6) increased with respect to the resonance fluorescence spectrum until eventually the latter spectrum was completely immersed inside the intense background fluorescence as shown in figure 4.5. This spectrum was produced when 100% of SO_2 concentration was expanded in the jet at 0.9

Table - 4.1 : Vibrational Analysis of for Resonance Fluorescence Spectrum of excited F - band (3021 Å).

Observed wavelength Å (Wavenumber cm^{-1})	Calculated wavelength Å (wavenumber cm^{-1})	Termination level at $^1A_1$
3130.2 (31937.9)	3129.93 (31940.66)	1 0 0
3150.5 (31732.1)	3150.71 (31730.00)	0 0 1
3233.7 (30915.6)	3234.07 (30912.09)	1 2 0
3246.0 (30798.5)	3246.21 (30796.48)	2 0 0
3268.0 (30591.1)	3267.87 (30592.40)	1 0 1
3289.0 (30395.8)	3288.66 (30398.94)	1 3 0
3290.5 (30382.0)	3290.89 (30378.39)	0 0 2
3301.0 (30285.3)	3301.04 (30284.98)	2 1 0
3347.5 (29864.6)	3347.03 (29868.81)	2 2 0
3371.0 (29656.4)	3370.61 (29659.86)	3 0 0
3416.0 (29265.8)	3416.17 (29264.31)	2 3 0

Continuation of Table - 4.1

Observed wavelength Å (Wavenumber cm^{-1})	Calculated wavelength Å (wavenumber cm^{-1})	Termination level at $^1A_1$
3430.0 (29146.3)	3429.39 (29151.53)	3 1 0
3442.5 (29040.5)	3442.83 (29037.72)	0 0 3
3464.0 (28860.2)	3463.53 (28864.21)	1 6 0
3477.0 (28752.3)	3476.66 (28755.15)	2 4 0
3490.5 (28641.1)	3490.15 (28643.98)	3 2 0
3504.0 (28530.8)	3503.99 (28530.84)	4 0 0
3567.5 (28022.9)	3567.15 (28025.68)	4 1 0
3580.0 (27925.1)	3579.78 (27926.81)	1 0 3
3604.5 (27735.3)	3603.99 (27739.22)	2 6 0
3608.0 (27708.2)	3608.03 (27708.17)	0 0 4
3617.0 (27639.4)	3616.87 (27640.45)	0 8 1

Continuation of Table - 4.1 :

Observed wavelength Å (Wavenumber cm^{-1})	Calculated wavelength Å (wavenumber cm^{-1})	Termination level at $^1A_1$
3644.0 (27434.6)	3643.56 (27437.95)	2 4 1
3647.0 (27412.1)	3647.35 (27407.45)	5 0 0
3672.0 (27225.4)	3671.82 (27226.80)	4 0 1
3685.0 (27129.4)	3685.45 (27126.13)	2 2 2
3715.0 (26910.3)	3715.40 (26907.46)	5 1 0
3727.0 (26823.7)	3726.90 (26824.37)	2 0 3
3740.5 (26726.9)	3740.11 (26729.67)	1 5 2
3757.0 (26609.5)	3756.95 (26609.84)	1 0 4
3767.5 (26535.3)	3768.10 (26531.13)	3 1 2
3787.0 (26395.2)	3788.26 (26389.94)	0 0 5
3798.0 (26322.2)	3797.52 (26325.39)	2 1 3

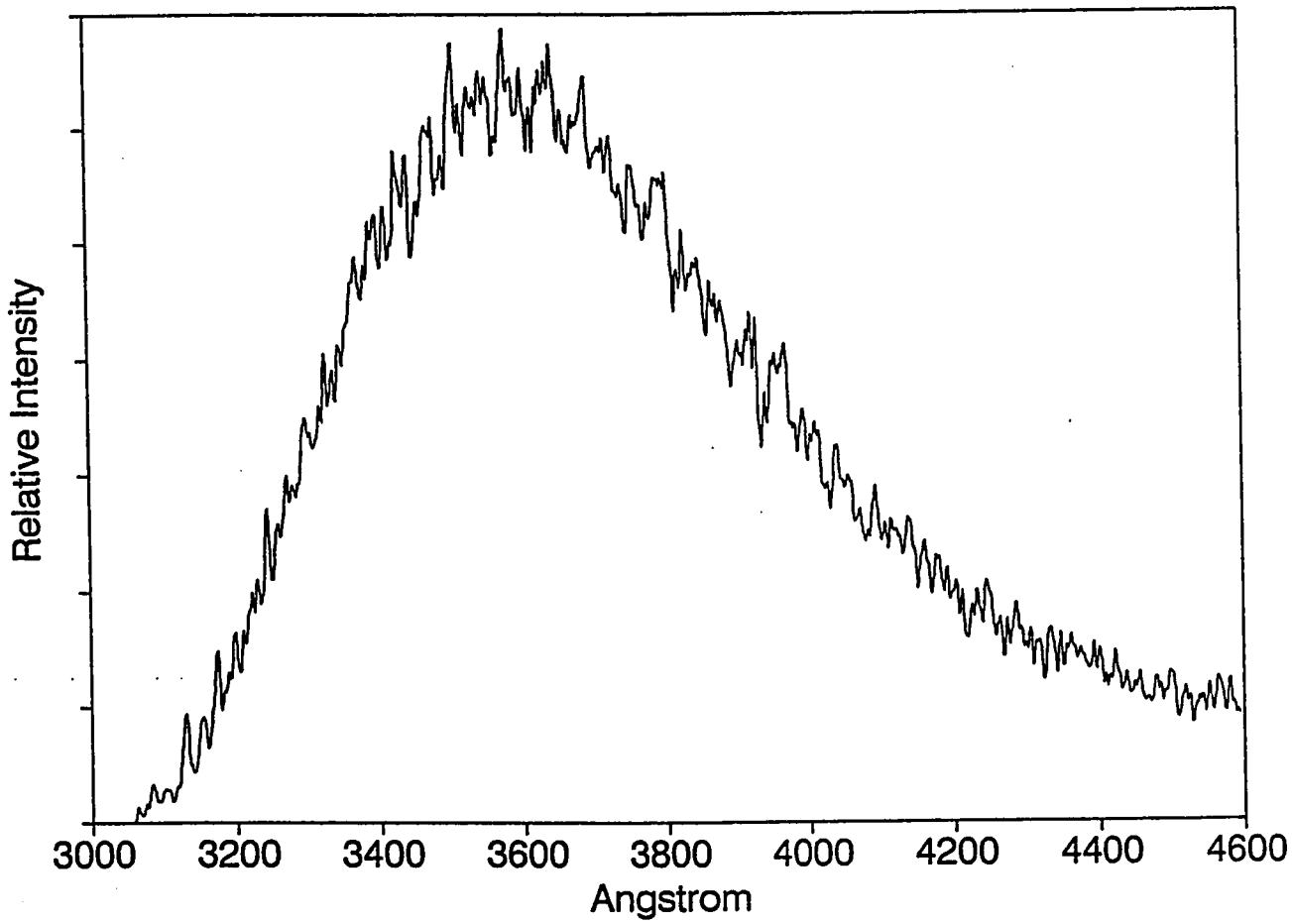

Figure: 4.5 Background fluorescence spectrum excited by the 3021Å wavelength with SO_2 concentration of 100%

atm stagnation pressure and 10 mm X distance. One may notice that the spectrum has a profile similar to the one recorded by Strickler and Howell[2] in a closed cell at 0.02 torr. At higher pressure the vibrational transition of the $^3B_1$ (0,0,0) —> $^1A_1$ band system in the 3800 -5000 Å region should also be observed similar to Strickler and Howell's result, when they used 0.97 torr pressure. Instead of achieving this condition we focused our attention on recording the phosphorescence spectrum at low pressure values, in which case the triplet molecules would not be vibrationally relaxed and the transitions from higher (ν_1, ν_2, ν_3) levels would also take place.

Phosphorescence spectra at such low SO_2 pressure are shown in figure 4.6. All of these spectra were produced at the excitation wavelength of 3021Å and keeping X fixed at 5 mm, but with different SO_2 concentration for each spectrum. The SO_2 concentration was 0.5% for 4.6c 0.3% for 4.6b and 0.1% for 4.6a, which correspond to the SO_2 pressure of 6 mtorr, 3.5 mtorr and 1.5 mtorr respectively and the total SO_2 + Ar pressure of 1.2 torr for all the three spectra.

These spectra could also be produced by using several other excitation wavelengths. Figure 4.7 shows an excitation spectrum recorded while monitoring the phosphorescence signal at 3721 Å transition and scanning the dye laser in 3045 - 3005 Å region. A laser wavelength corresponding to any peak on this spectrum could in principle produce the phosphorescence spectrum of figure 4.6, indicating that the triplet

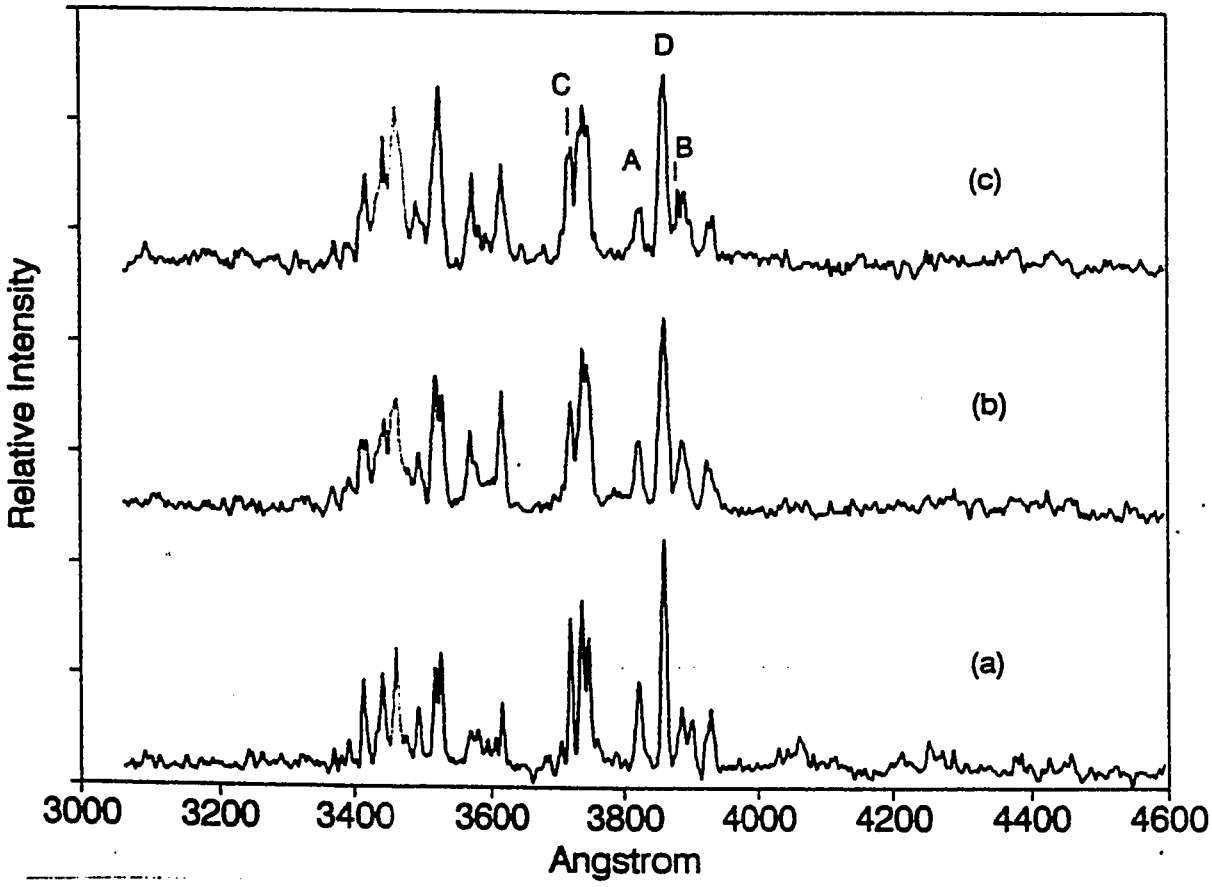

Figure : 4.6 Phosphorescence spectra excited by the 3021 Å laser radiation. The X distance was 5mm for all spectra and the SO_2 concentration was 0.1% for (a) 0.3% for (b) and 0.5% for (c).The bands marked A and B represent the $^3B_1$ (010) —> $^1A_1$(000) and $^3B_1$(000) —> $^1A_1$ (000) transitions respectively. Those marked C and D are assigned as the $^3A_2$ (130) —>$^1A_1$(001) and $^3A_2$(030)—>$^1A_1$ (001) transitions respectively

molecules can be formed by first order intersystem crossing at several upper singlet vibronic levels through equation 2.10.7. The asterisks on figure 4.7 identify the excitation wavelengths which we have actually used to reproduce the spectra in figure 4.6. The general feature of all reproduced spectra were the same except for slight different relative intensities of the transitions in each spectrum.

Almost all of the previous investigations of the wavelength resolved $^3B_1$ —> $^1A_1$ band system were reported in absorption only [35, 36]. The only reference known to us that shows this wavelength resolved band system in emission and also under low pressure conditions is reported by Caton and Gangadharan [10] whose results we use here for comparison. Even though their spectra did not extend below 3800 Å, a comparison can still be made for at least three key vibrational transitions. The peaks marked A and B in figure 4.6 and also in figure 1 of reference 10 refer to the $^3B_1$ (010) —>$^1A_1$ (000) transition at 3825 and $^3B_1$ (000) —>$^1A_1$ (000) transition at 3881 Å respectively. The peak marked C at 3721 Å is not covered in the spectral range of reference 10, but the D peak at 3858 Å can be clearly seen there. By examining the relative intensities of the marked peaks in figure 4.6, one may notice that the intensity of A transition decreases with respect to B transition as the SO_2 partial pressure is increased, while the intensities of C and D transitions with respect to each other are always more or less unchanging. This indicates that the equilibrium of ν_2 bending mode of $^3B_1$ has not yet been reached at SO_2 partial pressure of 6 mtorr,

while some sort of another equilibrated vibrational transition has already been in effect. It can be shown that the latter equilibrium is taking place for a vibrational mode of another electronic state and not for any of the other vibrational modes of the $^3B_1$ state by examining the relative intensity of the D transition.

In figure 1 of the reference 10 the intensity ratio I_B/I_A increased from a value less than 1 to a value larger than 1 as the pressure was increased from 3 mtorr to 10 mtorr. Within this pressure range the intensity of the D transition appears to be decreasing from a value that is relatively larger than A's intensity to one that is less than B's intensity. One may then at first sight conclude that D transition is some hot vibrational transition of $^3B_1 \rightarrow {}^1A_1$ system, however this is not exactly what we infer from our experiment. In figure 4.6 as the I_B / I_A ratio varies in the same range as above, the intensity of the D transition remains larger than the intensity of both of the A and B transitions, and seems to be independent of the pressure within the above specified range. This contradiction is indicative of a diffusive motion of molecules having different lifetimes, and is brought about by the way they were detected within the spectrometer's field of view. Under the condition of low pressure (or low SO_2 concentration in the supersonic jet case) not only the phosphorescence signal is weak but also the molecules have a chance to diffuse out and therefore in order to get a reasonable signal to noise ratio one resorts to adjusting the alignments of the exciting beam with respect to the detection

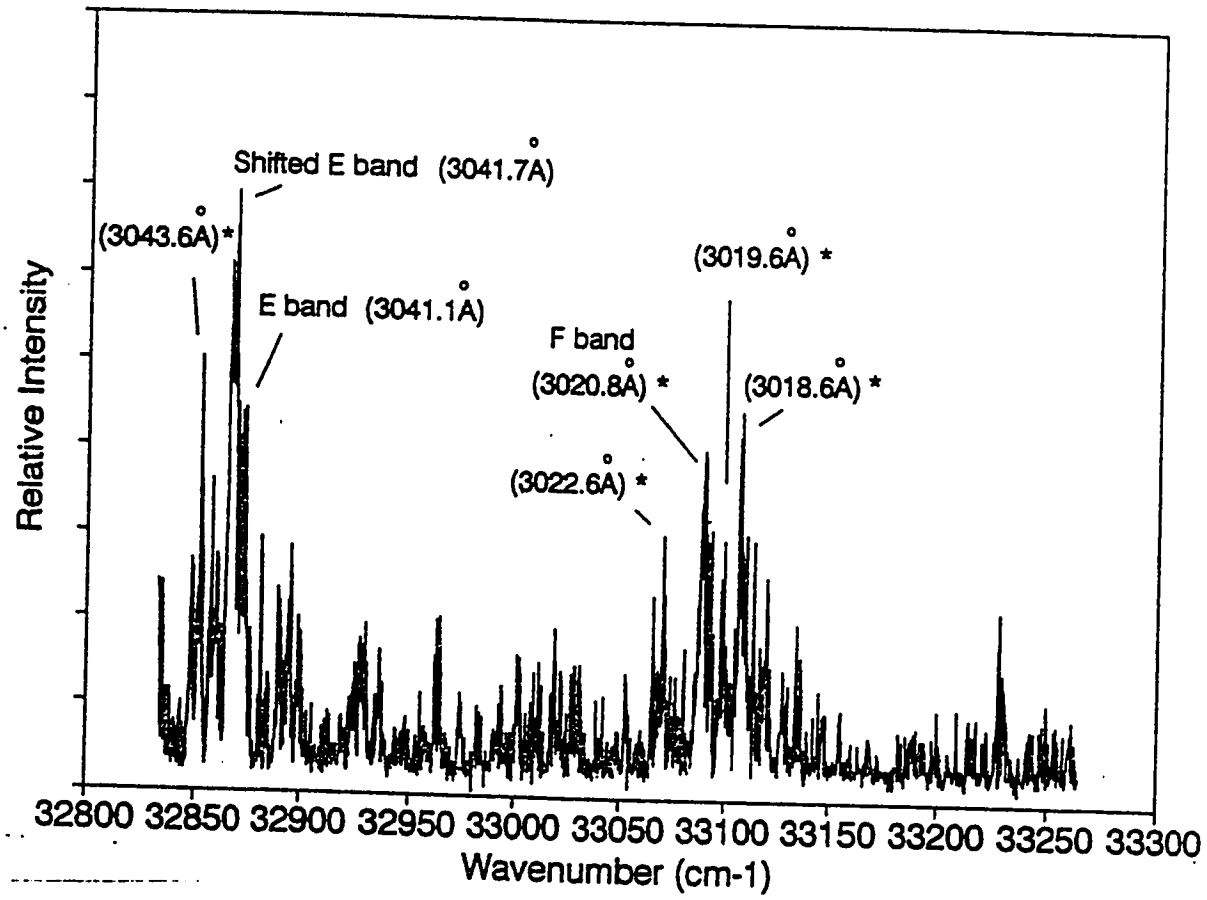

Figure : 4.7 Excitation spectrum produced by scanning the laser in the 3045 - 3005 Å region, while monitoring the phosphorescence signal at 3021Å (which corresponds to C transition of fig 4.5). The asterisks indicate the excitation wave lengths that were used to reproduce the phosphorescence spectrum in figure 4.6b

optics. A specie of molecule having a longer lifetime than another specie will diffuse farther before decaying and will have better chance to be detected at a greater distance between the spectrometer's field of view and the point of excitation. The upper level of the D transition then be assigned as belonging to an electronic state having a different life-time than the $^3B_1$ state, and that could only be the $^3A_2$ state according to theory.

The C transition whose energy is 955 cm^{-1} above the energy of the D transition is also assigned as a member of the $^3A_2 \rightarrow {}^1A_1$ system, since it is in equilibrium with the D transition in the pressure range of figure 4.6. As the SO_2 concentration was decreased further, the intensities of these two transitions (C and D) change noticeably with respect to each other as can be seen in figure 4.8. Here the SO_2 concentration was about 0.05% for 4.8a and < 0.05% for 4.8b corresponding to SO_2 partial pressures of 0.6 mtorr and, < 0.6 mtorr respectively. The equilibrium occurring in these two vibrational transitions in figure 4.6 has now become invalid at such low SO_2 partial pressures. Notice that by fixing the X distance the Ar partial pressure, which can be considered as equal to the total SO_2 + Ar pressure is always fixed. Therefore the role played by Ar gas in collision process, whether it enhances the production of the $^3A_2$ molecules or not, is always invariable and can not be responsible for the intensity variation of the C and D transitions.

A Perusal of Spectra in figure 4.8 will reveal that unlike the spectra of figure 4.6 there are several nearly equally spaced transitions

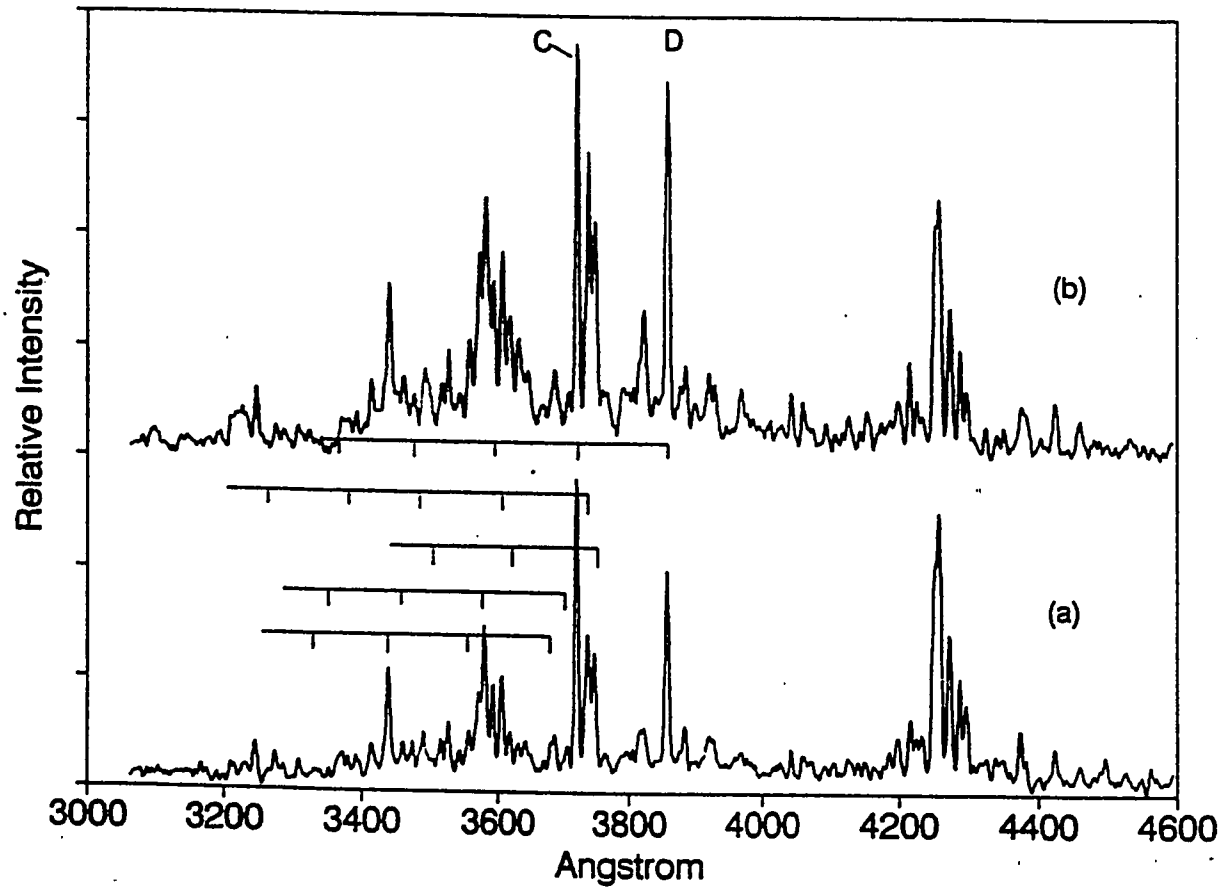

Figure : 4.8 Phosphorescence spectra excited by the 3021 Å radiation. The SO_2 concentration was 0.05% in (b) and , 0.05% in (a). The hoizandal lines in (a) point at five ν_1 progressions of the $^3A_2$ state.

present below 4000Å. The 3500 - 3700 Å region, in particular shows prominent and well resolved transitions that were not clear at the higher SO_2 pressure and serves as a linking members of five different progressions whose frequency separation equals to 955 cm^{-1}. According to Vickesland and Strickler [13], the 3500- 3700 Å is a region in which the $^3B_1 \rightarrow {}^1A_1$ transition showed far greater intensities than the one predicted from the Franck- Condon factors, when compared with the transitions occurring above 3700 Å which led them to propose that these bands were due to the perturbation by the states other than $^3B_1$. In their work on solid SO_2, Hochstrasser and Marchetti [37] also observed that the perturbation in absorption spectrum in the $^3B_1 \rightarrow {}^1A_1$ region and suggested that $^3A_2$ state may occur at about 3700Å. The above observations provide additional evidence that the spectra in figure 4.8 includes the progressions belonging to the $^3A_2 \rightarrow {}^1A_1$ which were previously not detected.

4.3 Vibrational Analysis of $^3A_2$

As mentioned before, in figure 4.8, below 4000Å we can notice equally spaced transitions of 955 cm^{-1} energy difference. Compared with the vibrational modes of other electronic states, the 955 cm^{-1} energy difference would be too big for considering it as the ν_2 mode of the $^3A_2$ state. Also because the progressions with a running quantum of the un symmetric mode ν_3 should have alternating strong - weak transitions that depend on whether the running quantum is odd or even, the 955 cm^{-1}

Table 4.2 : Five ν_1 progressions of $^3A_2$ showing the energy difference of about 955 cm^{-1}

Wavelength Å Wavenumber cm^{-1}	ΔE cm^{-1}	Wavelength Å Wavenumber cm^{-1}	ΔE cm^{-1}	Wavelength Å Wavenumber cm^{-1}	ΔE cm^{-1}
3858 (29913)		3748 (26673)		3736 (26759)	
	954		951		957
3721 (26867)		3619 (27624)		3607 (27716)	
	957		947		954
3593 (27824)		3499 (28571)		3487 (28670)	
	953				951
3474 (29171)				3375 (29621)	
	950				951
3363 (29727)				3270 (30572)	

Wavelength Å Wavenumber cm^{-1}	ΔE cm^{-1}	Wavelength Å Wavenumber cm^{-1}	ΔE cm^{-1}
3706 (26976)		3680 (27166)	
	957		955
3579 (27933)		3555 (28121)	
	952		949
3461 (28885)		3439 (29070)	
	948		943
3351 (29833)		3331 (30012)	

energy difference in figure 4.8 can not be for that mode either, and therefore it must be for zero order ν_1 vibrational mode. Therefore the vibrational equilibrium noticed in the $^3A_2$ state is interrupted as the equilibrium in the ν_1 vibrational mode. The member of progressions along with the energy separation are listed in table 4.2. It should be noted that the lower levels of the 5 progressions are not necessarily the same, and the transitions should obey the selection rule:

$$\Gamma\psi ev' \times \Gamma\mu \times \Gamma\psi ev'' = \text{ Totally symmetric.} \qquad (4.3.1)$$

where ψ_{ev}' and ψ_{ev}'' are the products of the electronic and vibrational wave functions in the upper and the lower levels, respectively, and μ is the dipole moment vector belongs to the C2v point group. In this the transitions involving the odd numbered quanta of the unsymmetric vibrational mode in the $^3A_2$ state (ν_3') will basically terminate into the levels involving the symmetric vibrational modes of the $^1A_1$ ground state i.e.ν_1'', ν_2'' and even numbered quanta of ν_3'' and vice versa. Other progressions that could be identified if figure 4.8 were those ones that belong to the ν_1'', ν_2'' modes of $^1A_1$ state. No other relatively long progressions of another $^3A_2$ mode could be untangled from the spectrum in figure 4.8a. This will indicate that the mechanism that leads to the population of $^3A_2$ state can be made possible by ν_1 activity only. However we found that an energy difference of about 417 cm^{-1} was common among several pairs of transitions suggesting that 417 cm^{-1} may be the zero order value for the ν_2 mode of $^3A_2$ state. The peaks that have the difference of

Table 4.3 : Some pairs of peaks showing the energy difference of about 417 cm^{-1} or the multiple of it, which is identified as the ν_2 mode of vibration of $^3A_2$.

Wavelength Å wavenumber cm^{-1}	ΔE cm^{-1}	Wavelength Å wavenumber cm^{-1}	ΔE cm^{-1}
3236 (27525)	408	3706 (26975)	1257 = 3 x 419
3579 (27933)	419	3541 (28232)	
3526 (28532)			

Wavelength Å wavenumber cm^{-1}	ΔE cm^{-1}	Wavelength Å wavenumber cm^{-1}	ΔE cm^{-1}
3921 (25496)	416	3806 (26266)	848 = 2 x 424
3858 (25912)	416	3687 (27115)	
3797 (36329)			

Table 4.4 : Tentative vibrational analysis for $^3A_2$--- $^1A_1$ system with the accuracy of 10 cm^{-1}. The 000- 000 transition is assumed to be 3842Å. Wavelengths are stated in air, while the wave numbers are stated in vacuum.

Transitions Å (cm^{-1}) Observed	Transitions Å (cm^{-1}) Calculated	$^3A_2 \rightarrow {}^1A_1$
3968 (25195)	3971.8 (25177)	011 - 200
3921 (25497)	3921.0 (25497)	020 - 001
3858 (25913)	3858.9 (25914)	030 - 001
3806 (26267)	3808.5 (26257)	111 - 120
3797 (26329)	3797.8 (26331)	040 - 001
3748 (26673)	3751.5 (26656)	031 - 110
3736 (26759)	3736.0 (26759)	021 - 100
3721 (26867)	3721.7 (26869)	130 - 001
3687 (27115)	3686.3 (27127)	131 - 120
3680 (27166)	3681.2 (27166)	311 - 140
3632 (27525)	3632.0 (27525)	101 - 010
3619 (27624)	3621.6 (27611)	131 - 110
3607 (27716)	3608.2 (27714)	121 - 100
3593 (27824)	3593.0 (27824)	230 - 001

Continuation of Table 4.4.

Transitions Å (cm^{-1}) Observed	Transitions Å (cm^{-1}) Calculated	$^3A_2 \longrightarrow {}^1A_1$
3579 (27933)	3578.8 (27942)	111 - 010
3555 (28122)	3560.9 (28082)	411 - 140
3541 (28233)	3541.3 (28238)	041 - 010
3526 (28352)	3526.2 (28359)	121 - 010
3514 (28450)	3513.4 (28462)	111 - 000
3499 (28572)	3500.6 (28566)	231 - 110
3487 (28670)	3488.0 (28669)	221 - 100
3474 (28777)	3474.7 (28779)	330 - 001
3461 (28885)	3460.5 (28897)	211 - 010
3439 (29070)	3443.8 (29037)	511 - 140
3375 (29621)	3375.6 (29624)	321 - 100
3363 (29731)	3363.1 (29734)	430 - 001
3351 (29833)	3349.8 (29852)	311 - 010
3331 (30013)	3334.2 (29992)	611 -140
3270 (30572)	3270.2 (30579)	421 -100

about 417 cm^{-1} and the multiple of 417 cm^{-1} are shown in table - 4.3. The prominent vibrational transitions appearing in the 4200 - 4400 Å region of figure 4.8represents the transition from high vibrational level in $^3A_2$, also possibly $^3B_1$ to high levels of $^1A_1$ in which the Franck-Condon factors are also favorable. It can be noticed that these transitions grow in intensity with respect to the transitions in the region below 3900 Å as the concentration is decreased implying that higher vibrational levels become more and more populated as the SO_2 pressure is decreased.

If we consider the $^3A_2$ (000) —> $^1A_1$(000) transition to lie near 3846 Å as pointed out in reference 1 and use the above values of ν_1 and ν_2 we can present a tentative analysis scheme for the spectrum in figure 4.8a based on equation 4.3.1. Such scheme is shown in table 4.4, where we have used the value 1063 cm^{-1} for ν_3' and 3842 Å for 000 -000 transition to get the best fit.

4.4 Formation Mechanism and internal conversion of $^3A_2$

It is clear then that, similar to the formation mechanism of $^3B_1$ molecules, the $^3A_2$ molecules are also formed by first order radiationless inter system crossing as in equation 2.10.7.

$$^1B_1(L) \xrightarrow{\text{inter system crossing}} {}^3A_2 \qquad (4.4.1)$$

According to Caton and Gangadharan [10], the ν_2 mode of $^3B_1$ state would eventually reach equilibrium at the pressure of about 30 mtorr in pure SO_2 gas at which I_A/I_B ratio reaches 0.2 . By looking at the I_A/I_B ratio in figure 4.6 and how it changes with SO_2 pressure, one may notice that the pressure condition of figure 4.6c are not far from achieving the vibrational equilibrium for ν_2 mode of $^3B_1$ state. Similarly by assuming that at at the concentration of 0.1% (1.5 mtorr of SO_2 pressure), the vibrational equilibrium in the $^3A_2$ state is achieved, one can consider that this vibrational equilibrium occurs more or less at about the same pressure condition at which the $^3B_1$ phosphorescence quantum yield is minimal according to Caton and Gangadharan. This latter phenomenon indicates that there is some sort of internal conversion must take place between the $^3B_1$ and $^3A_2$ states at high vibrational levels.

$$^3A_2 \xrightarrow{\text{internal conversion}} {}^3B_1 \qquad (4.4.2)$$

The rate at which this internal conversion is taking place and determination of the exact role played by Ar as a buffer gas in the enhancement of this process can not be determined from our work. Further spectroscopic and kinetic investigations are aimed at studying the quenching rate of $^3A_2$ state and the activation energy in the presence of Ar may provide a proper quantitative description for this process.

Assuming the validity of equation 4.4.2, one can attempt at explaining the phenomenon observed by Caton and Gangadharan [10], namely the upturn in the phosphorescence quantum yield at low SO_2 pressure, by considering the total formation rate of $^3B_1$ molecule. Besides equation 2.10.7 and equation 2.10.11, the $^3B_1$ molecules can also be formed by equation 4.4.2 especially at low SO_2 concentration when the higher vibrational levels $^3A_2$, which permit efficient internal conversion to $^3B_1$ levels, are still populated. For the sake of discussion, let us assume that the production rate of $^3B_1$ through intersystem crossing (equation 2.10.7) is constant in the pressure range of our experiment, and that one needs only to consider the production of $^3B_1$ through collision (equation 2.10.11) and through internal conversion (equation 4.4.2) to account for any change in the $^3B_1$ formation rate. At zero pressure the collision does not take place and therefore the total $^3B_1$ formation rate can be attributed to the internal conversion of $^3A_2$ (equation 4.4.2) only. As SO_2 partial pressure increases the production of $^3B_1$ through collision (equation 2.10.11) will add a contribution to the total $^3B_1$ formation rate, and at the same time the contribution through the internal conversion (equation 4.3.2) will decrease as the pressure is increased. The net balance of these two processes would then be a decrease in the total $^3B_1$ formation rate. This decrease in the formation rate will continue with the increased SO_2 pressure until the $^3A_2$ state reaches vibrational equilibrium, particularly for its ν_1 mode at 1.5 mtorr. After such equilibrium the contribution due to the internal

conversion will stabilize and the net formation rate of $^3B_1$ molecule will start increasing monotonously with the increased pressure due to the collisional processes (equation 2.10.11) alone. According to the tentative analysis in table 4.4, the energy region at which the internal conversion takes place efficiently is probably at 2000 - 4000 cm^{-1} above the 000 of the $^3B_1$ state. This is based on the observation that the ν_1 progression of $^3A_2 \longrightarrow {}^1A_1$ band system suffered intensity drop in 3500 - 3700 Å region as the pressure was increased.

CHAPTER - V

CONCLUSION

The work presented in this thesis offers a wavelength resolved study of $^3A_2$ - $^1A_1$ band system excited by absorption of 3021 Å laser radiation at very low partial SO_2 pressure. The identification of the $^3A_2$ -$^1A_1$ system was based on a noticed vibrational equilibrium occurring at a lower pressure than that at which the equilibrium of the ν_2' vibrational mode of the $^3B_1$ state occurs. Five progressions of the ν_1' mode of the $^3A_2$ state have been identified with the zero order energy separation of about 955 cm^{-1}. No relatively long progressions were detected for the ν_2' and ν_3' modes, but based on the tentative analysis scheme their zero order values could be estimated as 417 cm^{-1} and 1062 cm^{-1}, respectively. The production of $^3A_2$ molecule was found to be through radiationless intersystem crossing from $^1B_1$ state, and an indication of some sort of internal conversion from $^3A_2$ state to $^3B_1$ state was detected. A possible explanation for the upturn phenomenon in the phosphorescence quantum yield was also offered in the light of our results. Quantitative study of these proposed mechanism as well as other collision related parameters, however could not be determined from this work.

LIST OF SYMBOLS

$^1A_1$	:	Ground electronic state of C2v molecule.
$^1A_2$, $^1B_1$	:	Singlet electronic states.
$^1B_1(L)$	:	Long lived singlet state.
$^1B_1(S)$	:	Short lived singlet state.
$^3B_1$, $^3A_2$	:	Triplet states.
C2z	:	Rotation about z axis.
σ_v (XZ)	:	Reflection through XZ plane.
σ_v (YZ)	:	Reflection through YZ plane.
T_x, T_y, T_z	:	Translation symmetry.
R_x, R_y, R_z	:	Rotation symmetry.
ν_1, ν_2, ν_3	:	Three normal modes of vibration of SO_2.
H_{el}	:	Electronic hamiltonian.
M_e	:	Electronic transition moment.
ψ_e'	:	Electronic wavefunction of upper level.
ψ_e''	:	Electronic wavefunction of lower level.
μ	:	Dipole moment operator.
M_{ev}	:	Vibronic transition moment.
ψ_{ev}'	:	Vibronic wavefunction of upper level.
ψ_{ev}''	:	Vibronic wavefunction of lower level.
X_{ij}, Y_{ijk}	:	First order and second order anharmonic constant

ΔE	:	Energy difference between two energy levels.
h	:	Planck's constant.
M	:	Mach number.
M_T	:	Terminal value of mach number.
n	:	Molecular density.
X	:	Nozzle to laser distance.

REFERENCES

(1) J. Heicklen, N. Kelly, and K.Partymiller, Rev. Chem. Intermed., **3**,315 (1980) and refrences therein

(2) S.J. Strickler and D.B. Howell, J. Chem. Phys.**49**,1947, (1968)

(3) G. Herzberg, "Molecular Spectra and Molecular structure III, Electronic Spectra of poly atomic Molecules," Van Nostrand, Princeton, N.J. 1966.

(4) Y. Hamada and A.J. Merer, Can. J. Phys.,**57**, 1443 (1974)

(5) Y. Hamada and A.J.Merer, Can. J. Phys., **53**, 2555 (1975)

(6) H.D. Mettee, J.Chem. Phys., **49**, 1784 (1968).

(7) T. N. Rao, S.S. Collier, and J.G. Calvert, J. Am. Chem. Soc., **91** 1609 (1969)

(8) L.E. Brus and J.R. Mac Donald, Chem. Phys. Lett., **21**, 243 (1973)

(9) L.E. Brus and J.R. Mac Donald, J. Chem. Phys., **61**, 97 (1974)

(10) R.B. Caton and A.R. Gangadharan, Can. J. Chem., **52**, 2389 (1974)

(11) K.F. Greenough and A.B.F. Duncun, J. Am. Chem. Soc., **83**, 555 (1961)

(12) J.C.D. Brand, V. T. Jones and C. Di Lauro, J. Mol. Spectr. 45, 404 (1973) ; **40**, 616 (1971)

(13) J.P. Vikesland and S. J. Strickler, J. Chem. Phys., **60**, 660 (1974)

(14) E. Higazi, A.Hamdan, A. Dastageer, and F. Al - Adel, "Vibrational Analysis of $^3A_2$ —> $^1A_1$ phosphorescence of SO_2

(15) Y. Morino, M.Tonimoto and S. Saito, Acta Chemica Scandanavica A, **42**, 346 (1988)

(16) G. Nickless, "Inorgonic Sulphur Chemistry", Elevier Scientific pub. Co. 1968.

(17) J.M.Hollas, " Modern Spectroscopy", Jhon Wiley & Sons, 1992.

(18) J.I. Steinfeild, "Molecules and Radiation", MIt Press, 1985.

(19) E.B. Wilson, J.C. Decius, P.C. Cross, "Molecular Vibrations" Mc GraHill, 1955.

(20) Yamanouchi, S. Takuchi, and S.Tsuchiya, J. Chem. Phys. **92**, 4044 (1990).

(21) D.C. Harris, M.D. Bertolucci, " Symmetry and Spectroscopy", Oxford University Press.

(22) J.B. Coon R.E. De Wames and C. M. Loyd.,J. Mol. Spectr. **8**, 285 (1962).

(23) F. Al- Adel, A. Hamdan, O. Binbrek, and J.S. Baskin, Chem. Phys. Lett., 189, **23** (1992)

(24) A. Ficher, R. Kullmer and Demtroder, Chem. Phys. **83**,415 (1984)

(25) D.R. Bates, "Atomic and Molecular Processes", Academic Press, 1962.

(26) J.E. Kent, M.F. O' Dwyer, and R.J. Shaw, Chem. Phys. Lett., **24**, 221 (1974)

(27) R.J. Shaw, J.E. Kent and M.F. O'Dwyer, Chem. Phys., **18**, 155 (1976)

(28) R.J. Shaw, J.E. Kent, and M.F. O' Dwyer, Chem. Phys. **18**, 165 (1976)

(29) L.Stockburger, III , S. Braslavsky, and Heicklen, J. Photochem.,**2**, 15 (1973)

(30) W. Koechner "Solid State Laser Engineering", Springer- Verlag, New York, 1976

(31) B.B. Laud "Laser and Nonlinear Optics", Jhon Wiley & Sons, 1991.

(32) A.M. Hamdan (Master Degree Thesis) King Saud University Riyadh - Saudi Arabia. (1985)

(33) A.R Skinner and D.W. Chandler, Am. J. Phys., 48,8 (1980)

(34) Computer Program devoloped by Dr. Ezzat Higazi, Laser Research Lab, KFUPM, Saudi Arabia, 1992.

(35) N. Metropolis and H. Beutler, Phys. Rev., **57**, 1078A (1940)

(36) H.W. Sidebottom, C. C. Badcook, G. E. Jackson, J. G. Calvert, G.W. Reinhardt and E.K. Demon, Environm. Sci. Tech.,**6**, 72 (1972)

(37) R.M. Houchstrasser and Marchetti, J. Mol. Spectrosc., **35**, 335 (1970)